nature communications

Article

https://doi.org/10.1038/s41467-025-59734-x

Infant craniofacial diversity in Early Pleistocene *Homo*

Received: 20 August 2024

Accepted: 2 May 2025

Published online: 03 June 2025

Check for updates

José Braga [1,2] & Jacopo Moggi-Cecchi [3]

The adult craniofacial diversity of early Pleistocene *Homo* species is relatively well-documented, but its developmental foundations is hindered by the scarcity of infant specimens with preserved skeletal features. Here, we present evidence of craniofacial development in early Pleistocene *Homo* infants. This study focuses on a mandible (Omo 222-1973-2744) from the Lower Omo Valley in Ethiopia, attributed to *Homo habilis*, along with a mandible (KW 7000) from Kromdraai and a maxilla (DNH 83) from Drimolen, both in South Africa. We find that early *Homo* from southern Africa includes infant specimens with diagnostic facial features, with DNH 83 and KW 7000 uniquely combining both dental and skeletal evidence. Structural differences between the mandibles of Omo 222-1973-2744 and KW 7000 attributed to *Homo* aff. *H. erectus*, suggest that taxonomic diversity in early *Homo* was already evident in infancy. Furthermore, the unique combination of mandibular and dental features in these infants highlights the importance of integrating both dental and cranial morphology to identify early *Homo*.

Adult facial morphology (size and shape) serves as the primary basis for differentiating the three earliest recorded species commonly attributed to *Homo*[1–10]—*H. erectus, H. habilis*, and *H. rudolfensis*—during the Gelasian, the first stage of the Early Pleistocene (2.588–1.806 million years ago, Ma)[11], though some fossil attributions to the genus remain debated[1]. This period, marked by significant climatic fluctuations (as evidenced by Marine Isotope Stages—MIS—103 to 64[11]), predates the earliest secure evidence of *Homo* dispersal outside Africa[12] and concludes with the transition from normal to reversed polarity at the end of the Olduvai subchron (C2n). Fossils from this period, collectively referred to as 'early *Homo*', provide critical insights into the geographic distribution and early species diversity within the genus. The facial morphology of SK 847[10] from Swartkrans (South Africa) suggests the presence of either *H. erectus*[10] or a previously unrecognized *Homo* species[13] in southern Africa around 2 Ma. In eastern Africa, the AL 666-1 maxilla from Hadar (Ethiopia), is dated to 2.33 Ma[6] or between 2.3 and 1.9 Ma based on faunal evidence[14]. It suggests either an affiliation with *H. habilis*[6], or a distinct species that is incompatible with *H. habilis* or *H. rudolfensis* and more derived toward *H. erectus*[2,4]. Alongside the earliest evidence of the genus *Homo* at 2.8 Ma from Ledi-Geraru (Ethiopia), represented by the LD350-1 adult mandible[9], these discoveries highlight a deep-rooted species diversity within *Homo* before 2 Ma[4]. This emphasizes the need to further investigate the evolutionary processes that shaped distinct lineages within the genus during its earliest stage in Africa[4], particularly across its southern and eastern regions.

The distinct adult facial features observed among early *Homo* species include a flat incisor row retracted along the bi-canine line, the foreshortened subnasal region and premolar row characteristic of *H. rudolfensis*[5,7]; a more primitive mandibular arcade with a high 'robusticity' index (corpus width/height × 100), resembling *Australopithecus*[4], and elongated, subparallel tooth rows typical of *H. habilis*[4]; and the reduced and more diverging post-canine rows and continuous supraorbital torus found in *H. erectus*[10]. Notably, the enamel-dentine junction morphology largely retains the australopith condition in *H. habilis*[15]—including its holotype, the OH 7 subadult mandible[16]—and does not effectively classify key specimens with derived facial features, such as AL 666-1 from Hadar, Ethiopia[6], and SK 847 from Swartkrans, South Africa[10], as *Homo*[15].

[1]Centre for Anthropobiology & Genomics of Toulouse, University of Toulouse, Toulouse, France. [2]Evolutionary Studies Institute, University of the Witwatersrand, Johannesburg, South Africa. [3]Laboratori di Antropologia, Dipartimento di Biologia, Universita' degli Studi di Firenze, Firenze, Italy.
e-mail: jose.braga@univ-tlse3.fr

Here, we aim to investigate the facial features in early *Homo* infants, with two main objectives. First, we aim to understand how they differed from *Paranthropus* and *Australopithecus*. Second, we examine how developmental processes may have contributed to the deep-rooted species diversity in adult facial morphology within the human genus during the early stage of the Early Pleistocene[4]. A key challenge is determining whether adult facial differences among *Paranthropus* and *Australopithecus* and early *Homo* specimens resulted from developmental plasticity (i.e., environmental sensitivity of development)[17], or from canalized developmental patterns established early in ontogeny[18]. While dental microanatomy[19–23] and geochemistry[24] provide insights into life history and age-at-death, they are currently insufficient for distinguishing closely related taxa or capturing the full extent of species diversity in early *Homo*. The study of infant morphology may help determine which morphological differences between species are established by birth. However, such studies are constrained by the limited fossil record of early *Homo* infants—individuals before the emergence of their first permanent molars, or M1s—that preserve ontogenetically informative skeletal features (Fig. 1). To address this gap, we present the first developmental evidence on the facial skeleton of early *Homo* infants, comparing these data with older juvenile (KNM-ER 820) and subadult (OH 7) specimens from the same genus, as well as with *Paranthropus* and *Australopithecus* (Fig. 1, Box 1).

Our analysis includes a total of 15 infants and slightly older juveniles—individuals before the emergence of their second permanent molars—from eastern ($n = 5$) and southern Africa ($n = 10$), supplemented by limited observations of the OH 7 subadult. Despite the OH 7 mandible being highly fragmented and not representing an infant or young juvenile, it was included in some comparisons due to its significance as the holotype of *H. habilis* (Fig. 1). We primarily focus on three previously undescribed early *Homo* infant specimens from Early Pleistocene deposits: (i) the nearly complete maxilla DNH 83 from the Drimolen Main Quarry (South Africa) (Figs. 1, 2), likely dating to ~1.95 and 2.04 Ma[25,26], (ii) the KW 7000 mandible with symphysis from Kromdraai Unit P (South Africa) (Figs. 1 and 3), with a biochronological age predating 2 Ma[27], and (iii) the Omo 222-1973-2744 mandibular corpus from submember G-5 of the Shungura formation in the Lower Omo valley (Ethiopia)[28] (Figs. 1 and 4), dated to ~2.1–2.31 Ma[29] (Supplementary Note 1). These three early *Homo* specimens are compared with seven *P. robustus* (DNH 47, KW 6420, DNH 44, DNH 84, KW 9000, SK 3978, SK 62) and one *P. boisei* (KNM-ER 1477) infants, four slightly older juveniles with M_1s just erupted, including *P. robustus* (SK 61), *P. boisei* (KNM-ER 1820) and two *Homo* aff. *H. erectus* (KNM-ER 820 and KNM-ER 1507) (Fig. 1, Box 1, Supplementary Fig. 1). The KNM-ER 820 (*Homo* aff. *H. erectus*) and KNM-ER 1820 (*P. boisei*) specimens are dated to a period following the Gelasian stage, after 1.806 Ma[29] (Box 1). Moreover, although no fossils of *Australopithecus africanus* infants with taxonomically diagnostic skeletal features have been recovered, limiting opportunities for comparisons, we occasionally include two older juveniles (Taung and STS 2) and one subadult (MLD 2) in our analyses. The juvenile holotype from Taung (South Africa) has erupting M^1 roots that are nearly half complete, and the slightly younger STS 2 juvenile from Sterkfontein (South Africa) shows M^1 root formation just beginning. The MLD 2 subadult from Makapansgat (South Africa) is characterized by newly erupted M_{2s}. To compare these specimens, we reconstruct the 3D surface geometry of each original fossil using either micro-computed tomography (micro-CT or μCT) (KW 7000, Omo 222-1973-2744, KNM-ER 820, KNM-ER 1507, KW 9000, KW 6420, SK 3978, SK 62, SK 61, KNM-ER 1477, KNM-ER 1820, OH 7) or synchrotron radiation (DNH 83, DNH 47, DNH 44, DNH 84). Generalized procrustes analysis (GPA) and principal component analysis (PCA) are applied where feasible (Methods), acknowledging the fragmentary nature of the fossil record.

Results

Morphological descriptions

DNH 83 is the youngest early *Homo* specimen discovered to date that preserves skeletal morphology (Figs. 1 and 2, Box 1, Supplementary Notes 1 and 2, Supplementary Table 1, Supplementary Figs. 2 and 5, Supplementary Data 1, 2), with an age-at-death between 0.52 and 0.59 years[22]. This right (R) maxilla retains the nasoalveolar clivus, the nasal aperture, the infraorbital region, part of the orbital floor, the base of the zygomatic process and the hard palate (Figs. 1, 2). Its dental arch preserves the still erupting first deciduous molar (dm^1) with its three roots formed between half (stage $R^{1/2}$) and three-quarter (stage $R^{3/4}$) of formation (Methods), showing moderate wear that indicates functional occlusion for some time (Fig. 2). Four unerupted germs are preserved within the alveolar bone (Fig. 2, Box 1, Supplementary Data 2). The dental mineralization of DNH 83 is similar to that of the one-month older DNH 47 *P. robustus* infant[22,30] (Box 1). The three dental features that distinguish DNH 83 from *Paranthropus* and *Australopithecus* are found on the dm^1 and include: (i) a marked tuberculum molare on both the outer enamel surface (OES)[31] (Fig. 2b) and the enamel-dentine junction (EDJ) (Fig. 5), in contrast to all *Paranthropus* and *Australopithecus* specimens, where it is faint or absent[31]; (ii) the absence of a crista obliqua on the OES (and the corresponding crest at the EDJ) connecting the protocone and metacone (Fig. 5a, b), which is typically present in all *P. robustus* and *A. africanus* specimens (Fig. 5c–f); and (iii) mesiodistal (MD) versus buccolingual (BL) crown dimensions, which fall very close to OH 39, attributed to *H. habilis*[32] (Supplementary Data 2, Supplementary Note 2, Supplementary Fig. 2). The DNH 83 maxilla (Fig. 2, Supplementary Note 2) is more derived toward *Homo* than the DNH 47 and KW 9000 *P. robustus* infants[30]. Similar to *H. sapiens* infants, the premaxilla[33] of DNH 83 is early fused (Supplementary Fig. 4a, b) and anteroposteriorly short (c. 50% smaller than in DNH 47) (Supplementary Table 1, Supplementary Fig. 5), and the inferior orbital rim protrudes forward slightly (Fig. 2b) due to the advanced growth of the bony orbit[34] (Supplementary Fig. 5). Additional features include the posterior position of the anterior root of the zygomatic process of the maxilla relative to the plane of the orbit (Fig. 2b, Supplementary Fig. 5), the acute angle of the posterior pole of the nasoalveolar clivus where its contacts the vomer (Fig. 2c, Supplementary Fig. 4e, f), and its notable posterior retraction compared to the lateral margin of the nasal aperture (Fig. 2c, Supplementary Fig. 5, Supplementary Note 2). In anterior view, the nasoalveolar clivus of DNH 83 does not possess the typical *Paranthropus* smooth gutter running in the midplane, from the floor of the nose onto the clivus of adults[35] and infants[30]. In DNH 83 instead, there is a sharp angulation between the floor of the nose and the flat clivus (Fig. 2a).

The KW 7000 mandible is preserved from a break through the open crypt containing the developing crown of the left (L) permanent canine (C) (close but before stage of crown half complete, $Cr_{1/2}$) positioned close to the lower border of the mandible, to the opposite side and the empty crypt for the developing RM_1 (Figs. 1 and 3, Supplementary Figs. 6–8, Supplementary Table 1, Supplementary Data 2). KW 7000 retains the intact and unerupted Rdm_2 with its roots nearly reaching half-completion ($R_{1/2}$) (Fig. 3f). This mandible is the only early *Homo* infant that preserves the peri-symphyseal region. High-resolution computed tomography (micro-CT) data reveal the unerupted germs of the L and R $I_{1\text{-}2}$, and R C, at similar stages of development (stage $Cr_{3/4\text{-}C}$) (Fig. 3g, h). Given the general trend for maxillary developmental delay[34], the KW 7000 infant is very close in age with DNH 83. Dental features that ally KW 7000 with other fossils attributed to *Homo*, with clear distinctions from *P. robustus* (Supplementary Note 2) are on the unworn dm_2 and include the protoconid tip mesially placed to the metaconid[31], and the MD elongation of the crown[31] (Fig. 3i, Supplementary Data 2). In KW 7000, the RI_1 MD (6.0 mm) exceeds the upper limit of the observed range for *P. robustus* (4.95–5.90, $n = 8$)[36], while the I_2/I_1 MD diameter ratio of KW 7000 (1.05)

https://doi.org/10.1038/s41467-025-59734-x

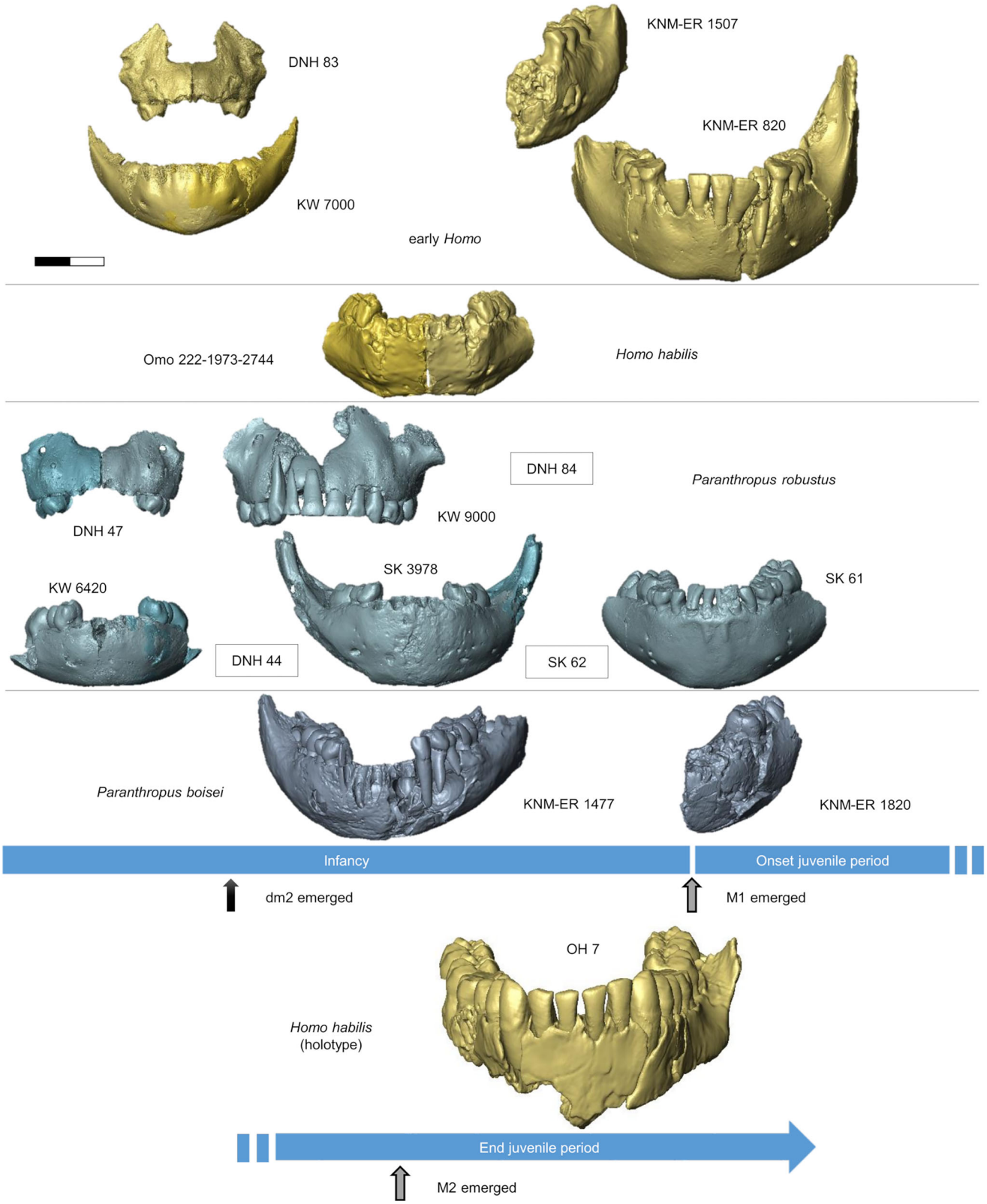

Fig. 1 | Facial skeletal remains of early *Homo* and *Paranthropus* infants and young juveniles. The early *Homo* (yellow color) and *Paranthropus* (gray–blue) specimens are rendered in 3D using the same scale and orientation. The 3D surfaces are reconstructed from micro-CT or synchrotron data of the original specimens. The mirror surface for DNH 83 (left), KW 7000 (left), Omo 222-1973-2744 (right), DNH 47 (right), KW 6420 (left), and SK 3978 (left) is illustrated for convenience. The specimens are arranged from left to right in order of increasing developmental age. The OH 7 specimen, with its second permanent molars erupted, is neither an infant nor a young juvenile but is illustrated at the bottom due to its importance as the holotype of *H. habilis*. For *Paranthropus robustus*, the more fragmentary specimens DNH 44, DNH 84, and SK 62 are not depicted.

BOX 1

Early *Homo* and *Paranthropus* infants that preserve sufficiently informative skeletal features

Specimen	Description	Taxon	Context and chronology
Infants (before or at dm2 emergence) (*n* = 11)			
DNH 83	Nearly complete R maxilla (except for parts of the zygomatic process, frontal process, and hard palate) with erupted Rdm^1 [$R^{1/2-3/4}$], and germs of RI^1 [$Cr^{1/2}$], RI^2 [Cr^i], R^C [$Cr^{1/4-1/2}$], dm^2 [R^i] (Figs. 1 and 2). Empty crypt for P^3. Age-at-death estimate: 0.52-0.59 years[22].	*Homo* sp.	South Africa (Gauteng), Drimolen Main Quarry, 1.95–2.04 million years ago (Ma)[25,26]
KW 7000	Mandible (including the symphysis) with the erupted Rdm_2 [$R_{1/2}$], and germs of R and LI_{1-2} [Cr_c], R and LC [$Cr_{1/2-3/4}$] (Figs. 1 and 3).	*Homo* aff. *H. erectus*	South Africa (Gauteng), Kromdraai, Unit P, Before 2 Ma[27]
DNH 47	R and L maxillary fragments with erupted $Rdi^{1,2}$ [R^c], L and Rdm^1 [$R^{1/2-3/4}$], Rdm^2 [$R^{i-1/2}$], and germs of $RI^{1,2}$ [$Cr^{i-1/2}$], RC [$Cr^{i-1/2}$], LM^1 [$Cr^{1/2}$] (Fig. 1). Empty crypt for P^3. Age-at-death estimate: 0.67-0.77 years[22].	*P. robustus*	South Africa (Gauteng), Drimolen Main Quarry, 1.95–2.04 Ma[25,26]
KW 6420	Mandible (including the symphysis) with erupted R and L (roots only) dm_1 [R_c-$A_{1/2}$], Rdm_2 [$R_{1/2}$], and germs of R and LI_{1-2} [$Cr_{1/2-3/4}$], R and LC [$Cr_{1/2}$], R and LP_3 [Cr_i] (Fig. 1). Empty crypt for P_4.	*P. robustus*	South Africa (Gauteng), Kromdraai, Unit P, Before 2 Ma[27]
DNH 44	R mandibular corpus (fractured near the midline of the symphysis) with erupted dc, dm_1, erupting dm_2 [$R_{1/2}$], and germs of RI_1-C [Cr_c], RM1 [Cr_c]. Age-at-death estimate: 1.70 years.		South Africa (Gauteng), Drimolen Main Quarry, 1.95–2.04 Ma[25,26]
KW 9000	Nearly complete R & L maxillae with erupted R and Li^1-dm^1, R and Ldm^2 [$R^{3/4-C}$], and germs of R and $LI^{1,2}$ [R^i], R and LC [$Cr^{1/2-3/4}$], R and LP^3 [$Cr^{1/2-3/4}$], R and LP^4 [Cr^i], RM^1 [R^i] (Fig. 1).	*P. robustus*	South Africa (Gauteng), Kromdraai, Unit P, Before 2 Ma[27]
SK 3978	Mandible (including the symphysis) with erupted L and Rdm_1 [R_c-$A_{1/2}$], L and Rdm_2 [$R_{3/4-c}$], and germs of L I_1 [$Cr_{1/2-3/4}$], R and LI_2 [$Cr_{1/2-3/4}$], R and LC [$Cr_{i-1/2}$], R and LP_3 [Cr_{cco}], LM_1 [$Cr_{3/4-c}$] (Fig. 1). Empty crypt for P_4.	*P. robustus*	South Africa (Gauteng), Swartkrans, Mb 1, 1.71–2.25 Ma[26]
Omo 222-1973-2744	L mandibular corpus (including part of the symphysis) with erupted dm_1, dm_2 [$R_{1/2-3/4}$], and germ of I_1 [Cr_c] (Figs. 1 and 4). Micro-CT data do not allow reliable assessments of development of germs.	*H. habilis*	Ethiopia, Lower Omo valley, Shungura Fm, sub-Mb G-5, 2.1–2.29 Ma[28]
DNH 84	Nearly complete L maxilla with erupted dm^1 [R^{res}], broken dm^2 [$A^{1/2}$], and germs of R and LI^1 [Cr^c], LC [$Cr^{3/4-c}$], LP^3 [$Cr^{1/2}$], LP^4 [Cr^{cco}], LM^1 [R^i]. Age-at-death estimate: 2.24 years[22].	*P. robustus*	South Africa (Gauteng), Drimolen Main Quarry, 1.95–2.04 Ma[25,26]
KNM-ER 1477	Mandible (including the symphysis) with erupted R and L dc-dm_2, and R and L germs of I_1 [Cr_c], I_2 [Cr_{sc}], C [$Cr_{3/4}$], P_3 [$Cr_{1/2}$], P_4 [$Cr_{1/2}$], M_1 [Cr_c] (Fig. 1).	*P. boisei*	Kenya (Eastern Turkana), Koobi Fora Fm, KBS channel complex, KBS Mb, 1.88–1.90 Ma[29]
SK 62	Mandible (including part of the symphysis) with erupted Ldi_2, R and LI_1 [$R_{1/2-3/4}$], LI_2 [$R_{1/2}$], R and Ldc-dm_2, and germs of R and LC [R_i], R and LP_3 [Cr_c], R and LP_4 [$Cr_{3/4-c}$], LM_1 [$R_{1/2}$], LM_2 [$Cr_{3/4-c}$]. Age-at-death estimate: 3.12 years.	*P. robustus*	South Africa, Swartkrans, Member 1, 1.71–2.25 Ma[26]
Slightly older juveniles (M1 emerging or just emerged) (*n* = 4)			
SK 61	Mandible (including the symphysis) with erupted R and Li_1-dm_2, and germs of R and LI_{1-2} [Cr_c], R and LC [R_i], R and LP_{3-4} [Cr_c], RM_1 [R_i] (Fig. 1).	*P. robustus*	South Africa, Swartkrans, Member 1, 1.71–2.25 Ma[26]
KNM-ER 1820	L mandibular corpus (fractured near to the midline of the symphysis) with erupted di_2-dm_1 (roots only), dm_2 and erupting M_1[Ri], and germs of I_2 [R_i], C [$Cr_{3/4-C}$], P_3 [$Cr_{3/4-C}$] (Fig. 1). Micro-CT data do not allow reliable assessments of development of P_4.	*P. boisei*	Kenya (Eastern Turkana), Koobi Fora Fm below Okote tuff complex, KBS Mb, 1.70 Ma[29]
KNM-ER 1507	L mandibular corpus fractured across the germ of C [R_i] with erupted dm_1-M_1, and germs of P_3 [R_i], P_4 [R_i], M_1 [R_c], M_2 [R_i] (Fig. 1).	*Homo* aff. *H. erectus*	Kenya (Eastern Turkana), Koobi Fora Fm, KBS Mb, 1.70–1.85 Ma[29]
KNM-ER 820	Mandible (including the symphysis) with erupted R and L I_{1-2}, R and L dc (roots only), R and L dm_1-M_1, and germs of R and L I_1 [R_c], I_2 [$R_{3/4}$], C [$R_{1/4}$], P_3 [$R_{1/4}$], P_4 [$R_{1/4}$] and M_2 [R_i]. (Fig. 1)	*Homo* aff. *H. erectus*	Kenya (Eastern Turkana), Koobi Fora Fm below Black Pumice Tuff, Okote Mb, 1.55–1.65 Ma[29]

The fossils are ranked based on their dental age, or histologically-derived ages-at-death estimates indicated in years. The dental developmental stages (see Methods) are indicated in brackets. R, right; L, Left. Fm, Formation, Mb, Member.

https://doi.org/10.1038/s41467-025-59734-x

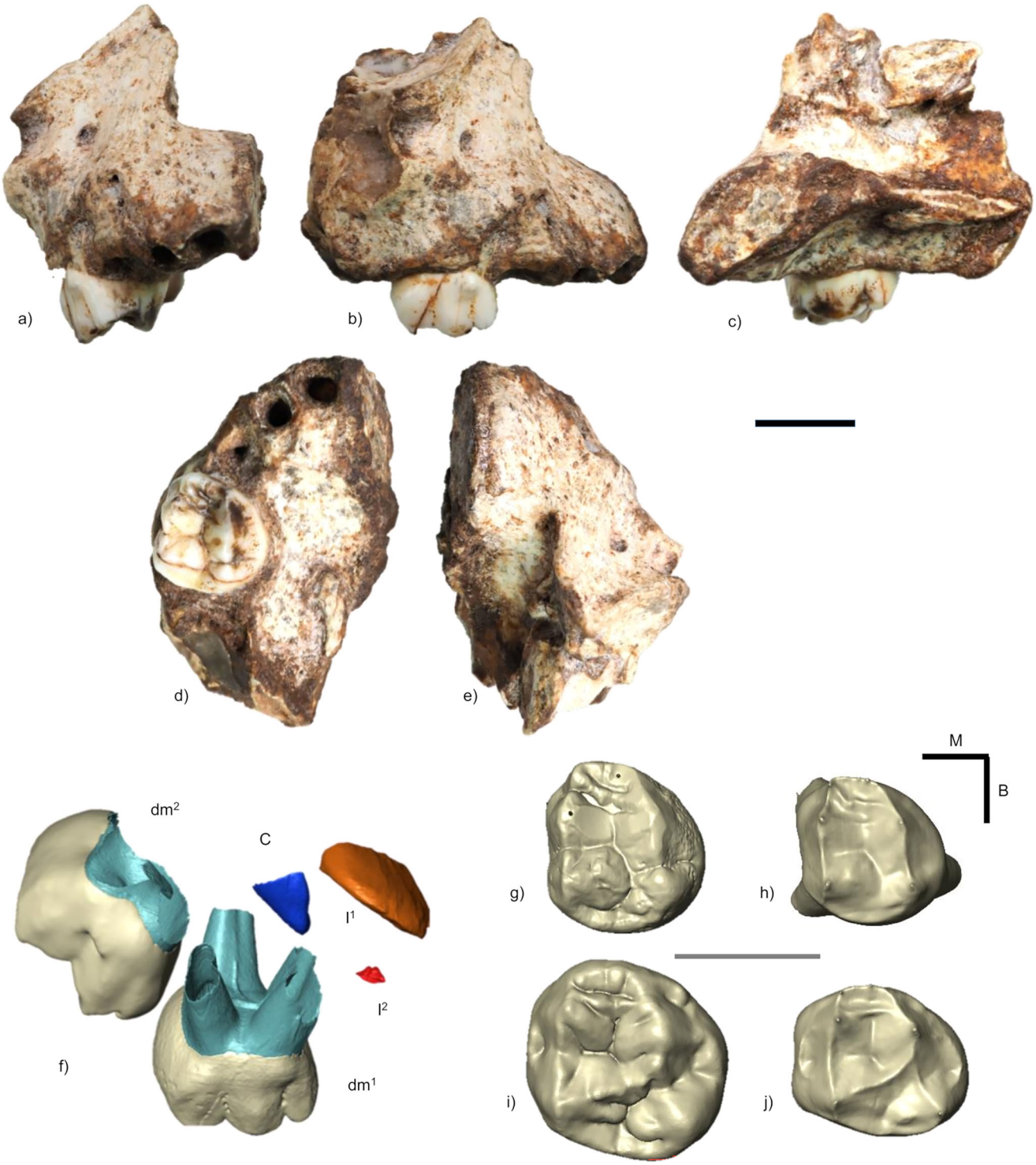

Fig. 2 | The DNH 83 right maxilla. The specimen is shown, with the dm^1 in position, in **a** anterior, **b** lateral, **c** medial, **d** inferior, and **e** superior views. Dental development (**f**) with the 3D models of the dm^1 (slightly less than half of its three roots formed) and the germs of the dm^2 (root initiation), permanent lateral (in red) and central (in brown) incisors, and permanent canine (in dark blue), in lateral view. The dm^1 (**g**, **h**) and dm^2 (**i**, **j**) were rendered in 3D with the outer enamel surface (OES) (**g**, **i**) and enamel-dentine junction (EDJ) (**h**, **j**) in occlusal views. Orientation is indicated by labeling one corner with the abbreviations M (mesial) and B (buccal). Scale bars, 1 cm.

falls notably below the lower limit of the *P. robustus* range (ranging from 1.11 in SK 34 to 1.18 in SK 23; 1.12 in KW 6420 from Kromdraai Unit P). This discrepancy is attributed to the typically small MD of the I_1 in *P. robustus* and its relatively lower value compared to the I_2. In KW 7000, the occurrence of several mammelons on the $I_{1\text{-}2}$ incisal edges show similarities with the *Homo* SKX 2354/5/6 specimen from Swartkrans[37]. This feature is not present in *Paranthropus*[36,38]. The primitive morphology of the KW 7000 developing crown of the C germ is noteworthy because the central part of its lingual face shows a marked median ridge with a very sharp edge departing from the cusp tip. This condition differs from *Paranthropus* which has a slight ridge, and is more similar to *A. afarensis* with a strong lingual ridge (e.g., AL 400-

https://doi.org/10.1038/s41467-025-59734-x

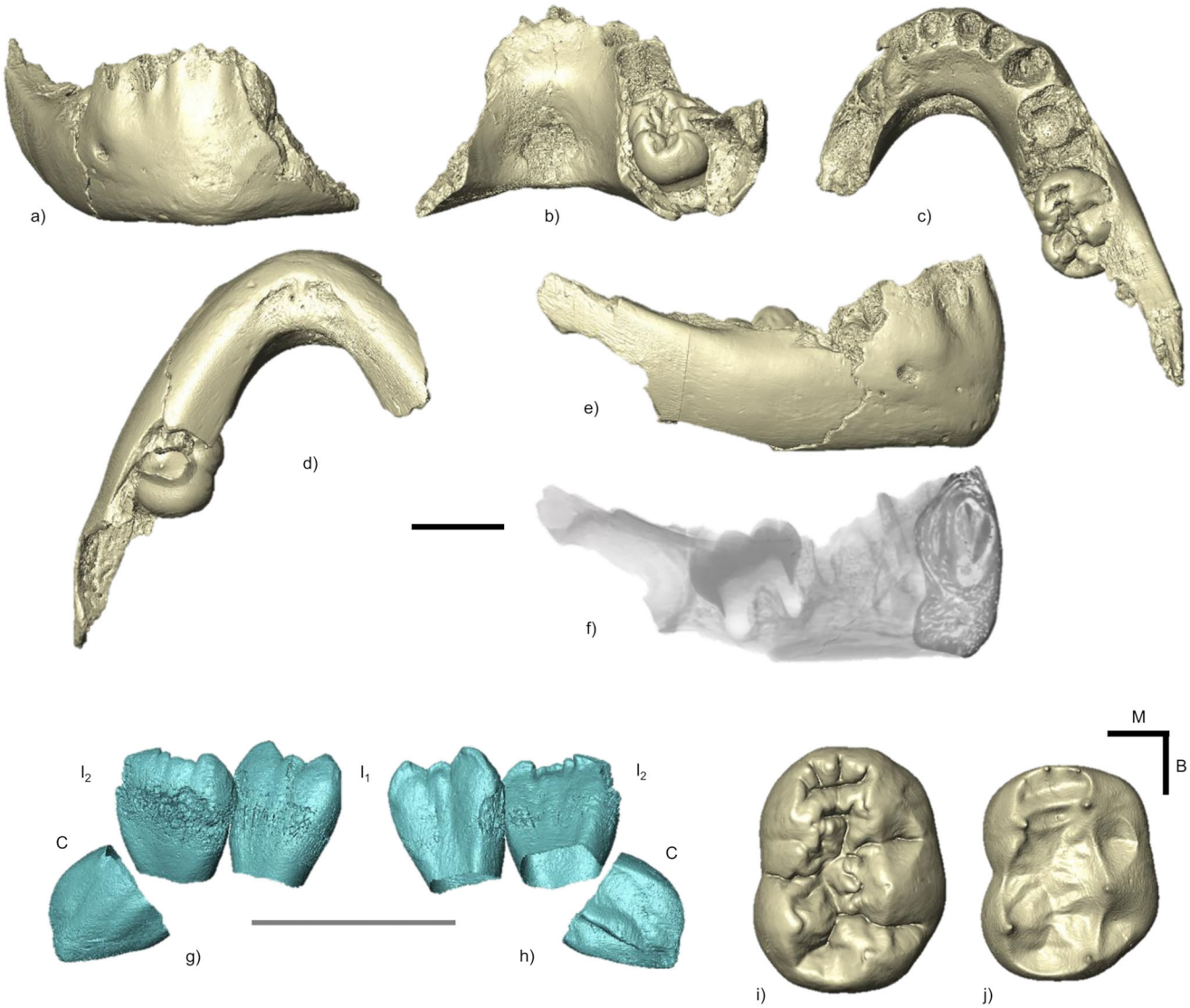

Fig. 3 | The KW 7000 mandible. The 3D model of the KW 7000 specimen was reconstructed from micro-CT data and shown in anterior (**a**), posterior (**b**), superior (**c**), inferior (**d**), and right lateral (**e**) views, with the dm_2 in position. The volume rendering of the mandible displayed in right lateral view (**f**) alongside the micro-CT slice of the symphysis in the mid-sagittal plane. The 3D models of the germs of the right permanent lateral (I_2) and central (I_1) incisors, and the right permanent canine (C) shown in buccal (**g**) and lingual (**h**) views. The KW 7000 right dm_2 (**i**, **j**) rendered in 3D with the OES (**i**) and EDJ (**j**) in occlusal views. Orientation is indicated by labeling one corner with the abbreviations M (mesial) and B (buccal). Scale bars, 1 cm.

1a,b)[39] and to *A. africanus* (e.g., Sts 51)[40]. The symphyseal axis forms an angle of ~104° with the basal plane (Supplementary Table 2), with a moderately prominent convex mental surface inferiorly, but no true chin (Fig. 3a). The inferior symphyseal surface is dominated by elongated geniohyoid depressions that are positioned anteriorly (Fig. 3d, Supplementary Fig. 7a). In contrast, these depressions are located along the posterior edge of the inferior symphyseal surface in the KW 6420 and SK 3978 *P. robustus*[30] and the KNM-ER 1477 *P. boisei* infants (Supplementary Fig. 7b–e). The KW 7000 mandibular corpus is ~20% and 47–55% smaller than the KW 6420 *P. robustus*[30] and the KNM-ER 1477 *P. boisei*[38] infants, respectively (Supplementary Table 2, Supplementary Fig. 6).

The Omo 222-1973-2744 L mandibular corpus is preserved from a break near to the midline of the symphysis through the exposed distal side of dm2 (Figs. 1 and 4, Supplementary Fig. 6, Supplementary Table 2, Supplementary Data 2, Supplementary Notes 1 and 2). Omo 222-1973-2744 is not yet described, except for its erupted $dm_{1\text{-}2}$ crowns, which have led to its attribution to *H. habilis*[31]. This fossil represents a developmentally slightly older individual than KW 7000. The germ of the I_1 is nearing crown-completion (Cr_c), while the development of the exposed distal root of the erupted dm_2 ranges from half to three-quarters completion ($R_{1/2\text{-}3/4}$) (Box 1). Due to insufficient tissue distinction in the micro-CT data, reliable assessments of the development of the other germs are not possible. At the level of the empty alveolus for the deciduous canine, a prominent jugum dominates the lateral aspect of the corpus, creating a noticeable swelling that demarcates it from the peri-symphyseal region and a squared-off incisor/canine row (Fig. 4a, d, e). In Omo 222-1973-2744, the symphyseal axis forms an angle of approximately 119° with the basal plane (Fig. 8e, f, Supplementary Table 2). In comparison to KW 7000, the post-incisive planum is about 50% shorter (Fig. 4, Supplementary Fig. 6).

Morphometric comparisons

We gain insights into the growth and development of the infant early *Homo* maxilla (DNH 83). Assessing how this fossil differs from *Paranthropus* and *Australopithecus* is challenging due to the absence of sufficiently preserved fossil infants from this group, with the notable

https://doi.org/10.1038/s41467-025-59734-x

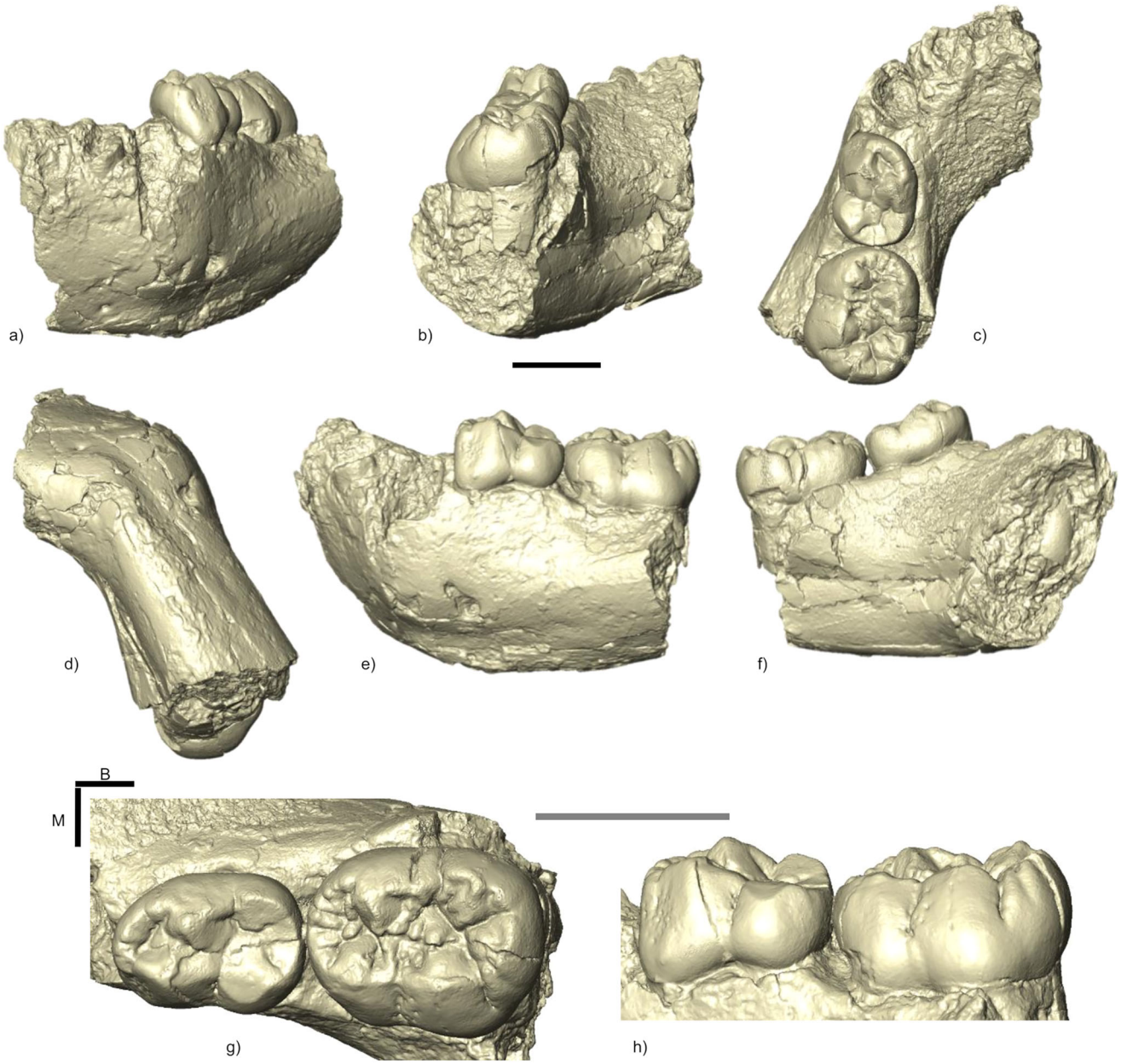

Fig. 4 | The Omo 222-1973-2744 mandibular corpus. The 3D model of the Omo 222-1973-2744 left mandibular corpus reconstructed from micro-CT data and shown in anterior (**a**), posterior (**b**), superior (**c**), inferior (**d**), left (**e**), and right (**f**) views, with the dm_1 and dm_2 in position. The left dm_1 and dm_2 were rendered in 3D with the OES in occlusal (**g**) and buccal (**h**) views. Orientation is indicated by labeling one corner with the abbreviations M (mesial) and B (buccal). Scale bars, 1 cm.

exception of *P. robustus* infants (DNH 47 and KW 9000)[30]. A PCA of 23 Procrustes landmarks and semi-landmarks coordinates (Methods, Supplementary Fig. 9) summarizes maxillary variation, taken on DNH 83, DNH 47, KW 9000, *H. sapiens* infants, and the slightly older *A. africanus* juvenile from Taung (Fig. 6, Supplementary Note 3). The first principal component (which captures 28.6% of variance) separates *H. sapiens* from DNH 83, *Paranthropus,* and *Australopithecus* (Fig. 6a, b). The most notable displacements in *H. sapiens*, compared to DNH 83, *Paranthropus* and *Australopithecus*, include the antero-posterior contraction of the nasoalveolar clivus (landmarks 8 to 14) along with the development of the anterior nasal spine (landmark 11) (Supplementary Fig. 9) (Fig. 6b, c). Additionally, there is a postero-superior shift of both the base of the lateral margin of the nasal aperture (landmark 15) and the alveolar border (landmarks 1 to 7) (Supplementary Fig. 9) (Fig. 6b, c). Compared to *P. robustus* and *A. africanus*, the facial morphology of the DNH 83 early *Homo* infant differs only along PC3, which accounts for 15.8% of the variation (Fig. 6b), compared to 18.9% for PC2 (Fig. 6a). Compared to the DNH 47 *P. robustus* infant, the most notable displacement in DNH 83 involves the backward shifting of the nasoalveolar clivus (primarily the premaxilla) (landmarks 8 to 14, Supplementary Fig. 9) relative to the lateral margin of the nasal aperture (landmark 15, Supplementary Fig. 9) (Fig. 6d).

Two PCAs of Procrustes landmark and semi-landmarks coordinates (Methods) reveal differences in the shape of the mandibular symphysis among KW 7000, Omo 222-1973-2744, *Homo* aff. *H. erectus* (KNM-ER 820), *P. robustus* ($n = 5$), *A. africanus* (MLD 2), and *H. sapiens* infants ($n = 46$) (Fig. 7). Regrettably, the damage to the basal aspects of their symphyses prevented the inclusion of the Taung juvenile[41] and the OH 7 subadult[4,16] in these analyses. In a first PCA, 50 semi-landmarks were used along the mid-sagittal plane of the symphysis to

https://doi.org/10.1038/s41467-025-59734-x

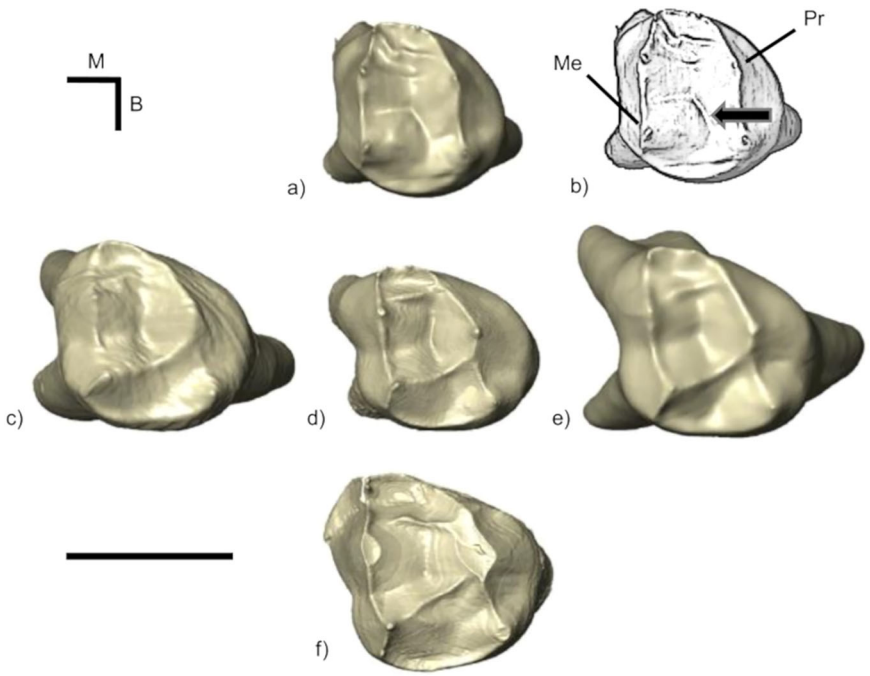

Fig. 5 | The dm^1 enamel-dentine junction in DNH 83, *Paranthropus robustus*, and *Australopithecus africanus* infants. 3D renderings (**a**, **c**–**f**) and a sketch (**b**) of the right dm^1 EDJ in occlusal view are shown for the early *Homo* DNH 83 infant (**a**, **b**), the *P. robustus* infants DNH 47 (**c**), DNH 84 (**d**, mirrored to the right) and KW 9000 (**e**), as well as the *A. africanus* juvenile STS 2 (**f**, mirrored to the right). The DNH 83 dm^1 EDJ (**a**, **b**) exhibits a marked groove (black arrow) between the dentine tips of the protocone (**b**, Pr) and metacone (**b**, Me). This ridge replaces the crest that typically connects these two tips in *P. robustus* and *A. africanus* specimens (**c**–**f**). Orientation is indicated by labeling one corner with the abbreviations M (mesial) and B (buccal). Scale bar, 1 cm.

compare the mandible of the KNM-ER 820 *Homo* aff. *H. erectus* infant with both KW 7000 and Omo 222-1973-2744 (Fig. 7a), despite the presence of a vertical crack between the left I_2 and d_c in the former specimen. Due to this damage, KNM-ER 820 could not be included in a second PCA that utilized 120 semi-landmarks evenly distributed across the symphyseal surface (Fig. 7c, Methods). In both analyses, PC1 (accounting for 62.1% and 60.3% of the variation, respectively) explains a much greater proportion of the total variance compared to PC2 (Fig. 7a, c). This indicates that the main source of variation among the specimens is captured primarily by PC1 which revealed significant differences (with a Monte-Carlo permutation test at $p < 0.001$) in symphyseal shape between KW 7000 and *H. sapiens* on one side, and Omo 222-1973-2744, *P. robustus*, and *A. africanus* on the other (Fig. 7a, c) (Methods). The mid-sagittal symphyseal shape of KNM-ER 820 and KW 7000 falls within the variation range observed in *H. sapiens* infants (Fig. 7a), where the vertical orientation remains constant throughout fetal and early postnatal development[42]. Interestingly, the mid-sagittal profile (Fig. 7a) and the surface (Fig. 7c) of the symphysis in Omo 222-1973-2744 lie within (Fig. 7a) or just outside (Fig. 7c) the documented variation range for *P. robustus* infants along PC1. The most negative PC1 values (accounting for 62.1% of the variation) correspond to a symphysis that slopes antero-inferiorly from the anterior alveolar border to the base, combined with an incurvatio mandibulae anterior (Fig. 7b). This distinctive mentum osseum is absent in the *H. sapiens* infants with the most positive PC2 values, as well as in both KNM-ER 820 and KW 7000. The primary difference between KNM-ER 820 and KW 7000 lies in the anterior and posterior aspects of the symphysis. In KW 7000, the anterior aspect does not slope antero-inferiorly as in KNM-ER 820, and the planum alveolare is short, with the superior transverse torus positioned well above the mid-height of the symphysis. In contrast, KNM-ER 820 has a long, sloping planum alveolare extending from the alveolar border to the superior transverse torus, which is located well below the mid-height of the symphysis (Fig. 7b). The extremes along PC2 are represented by *H. sapiens* infants who primarily differ in the posterior symphyseal morphology and the presence or absence of a chin (Fig. 7b). The mid-sagittal symphyseal shape of the Omo 222-1973-2744 specimen differs from that of KW 7000 primarily due to the markedly receding mandibular symphysis in the former (Supplementary Fig. 7). This morphology is also observed in *P. robustus* infants (SK 62 and KW 6420) and the *A. africanus* juvenile MLD 2, which exhibit the most positive PC1 values (Fig. 7b). The pronounced difference in symphyseal shape between the KW 7000 infant and the Omo 222-1973–2744 juvenile (Supplementary Fig. 7a, b, e–h) is also evident from their clear separation along PC1 (accounting for 60.3% of the variation) in the second PCA based on the symphyseal surface (Fig. 7c). KW 7000 falls within the variation range observed in *H. sapiens* infants, while the more positive PC1 values for the Omo 222-1973-2744 juvenile, MLD 2 and *P. robustus* infants correspond to a markedly receding mandibular symphysis (Fig. 7d). The KNM-ER 1477 *P. boisei* infant could not be included in this analysis due to its fragmentary symphysis (Fig. 1, Supplementary Fig. 6v). However, the angle between its axis and the basal plane (ASYM) (Methods) appeared very close to that of *P. robustus* juveniles (Supplementary Table 2).

We also performed a PCA of seven mandibular indices and one angle (Methods, Fig. 8a–d, Supplementary Table 2) in order to identify the features that had the most significant roles in overall mandibular morphology and robusticity index among our fossil sample. The correlation circle illustrates how the eigenvalue of each variable (Fig. 8e) is correlated to either PC1 or PC2 (Fig. 8e, f). Robusticity at dm_1 (WHdm1) and d_c (WHdc, Fig8b) is negatively correlated with symphyseal robusticity (HDSY, Fig. 8b), with all three variables showing the strongest correlation with PC1 (Fig. 8e). These variables appear to be independent of indices representing arcade shape, ALR and BRR (Fig. 8d, Methods), which shows the highest correlation with PC2. KW 7000 is distinct from all other specimens, including the Omo 222-1973-2744 juvenile (which falls within the variability range observed for *P. robustus* infants) along PC1, which accounts for 50.6% of the variation

https://doi.org/10.1038/s41467-025-59734-x

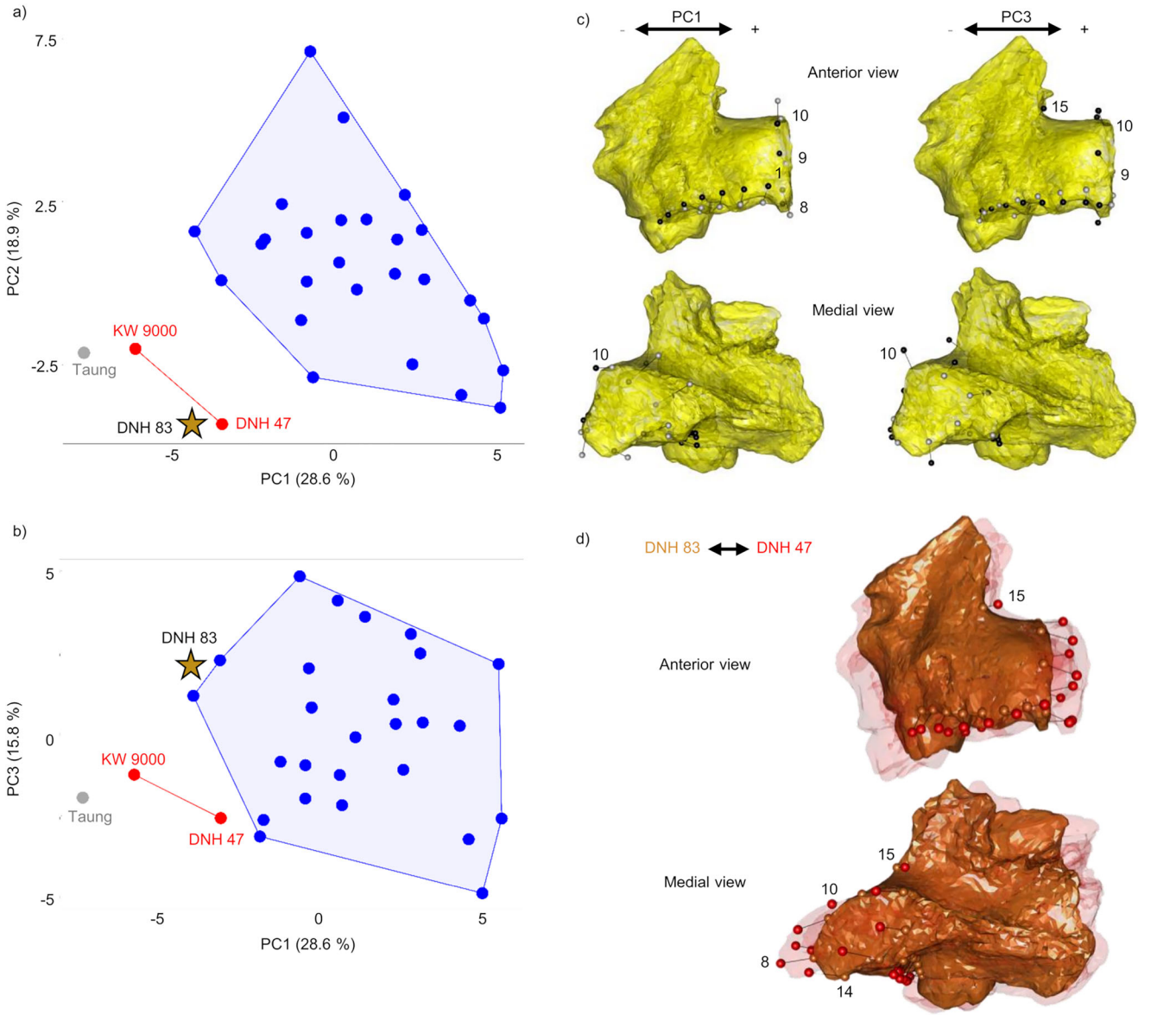

Fig. 6 | Morphometric comparisons of the DNH 83 maxilla with *Paranthropus robustus*, *Australopithecus africanus* and *Homo sapiens* infants. Plots of principal components (PCs) 1 and 2 (**a**), and 1 and 3 (**b**) describing the differences in maxillary shape between DNH 83 (brown star), *P. robustus* infants DNH 47 and KW 9000 (in red), the *A. africanus* holotype specimen from Taung (in gray), and *H. sapiens* infants (in dark blue). Variations within taxa are represented as convex polyhedra that enclose the corresponding points. **c** Landmarks, semi-landmarks, and vectors depicting shape changes corresponding to PC1 and PC3 are shown in anterior and left lateral views, superimposed on the mean shape (in yellow), which represents DNH 83 warped to the mean configuration of landmarks. The numbering of landmarks and semi-landmarks corresponds to the descriptions provided in the Methods section. The vectors (black segments) represent the displacement of landmarks and semi-landmarks from positions associated with the lowest values of PC1 and PC3 (in gray) to those corresponding to the highest values along these PCs. **d** The same vectors and views as in (**c**) are used to illustrate the displacement of landmarks and semi-landmarks from the positions associated with DNH 83 (landmarks in light brown) to those of DNH 47 (landmarks in red), superimposed on DNH 83 (in dark brown) and DNH 83 warped to DNH 47 (in transparency and in red).

(Fig. 8f). This distinction highlights a lower symphyseal robusticity index in the KW 7000 infant. Among the *P. robustus* specimens, SK 3978 and KW 6420—the two youngest in the sample—exhibit the most contrasting symphyseal robusticities, with SK 3978 having the most negative PC1 value in this sample and KW 6420 the most positive (Fig. 8f). In contrast, ER 820 is distinct from all other specimens, including *P. robustus*, along PC2, which accounts for 23.6% of the variation, emphasizing the lengthening of the mesiodistal diameter of its di1-di2 alveoli (ALR) (Fig. 8d, f, Methods).

In a PCA of 75 Procrustes landmark and semi-landmark coordinates representing the EDJ of the dm_2 (Methods), the morphology of the KW 7000 infant aligns closely with the variation observed in *P. robustus* ($n = 8$) (Fig. 9a). Specifically, along both PC1 and PC2, KW 7000 occupies an intermediate position relative to the extreme values of *P. robustus* specimens. Thus, the dm_2 EDJ morphology does not distinguish KW 7000 from *P. robustus*.

Discussion

Craniofacial development in early *Homo* infants

A century after the discovery of the iconic australopith juvenile from Taung (South Africa)[41], the evidence presented here highlights the importance of integrating dental and skeletal data from infant fossils for understanding the developmental biology, anatomy and taxonomy of early *Homo*. It has been proposed that developmental plasticity

https://doi.org/10.1038/s41467-025-59734-x

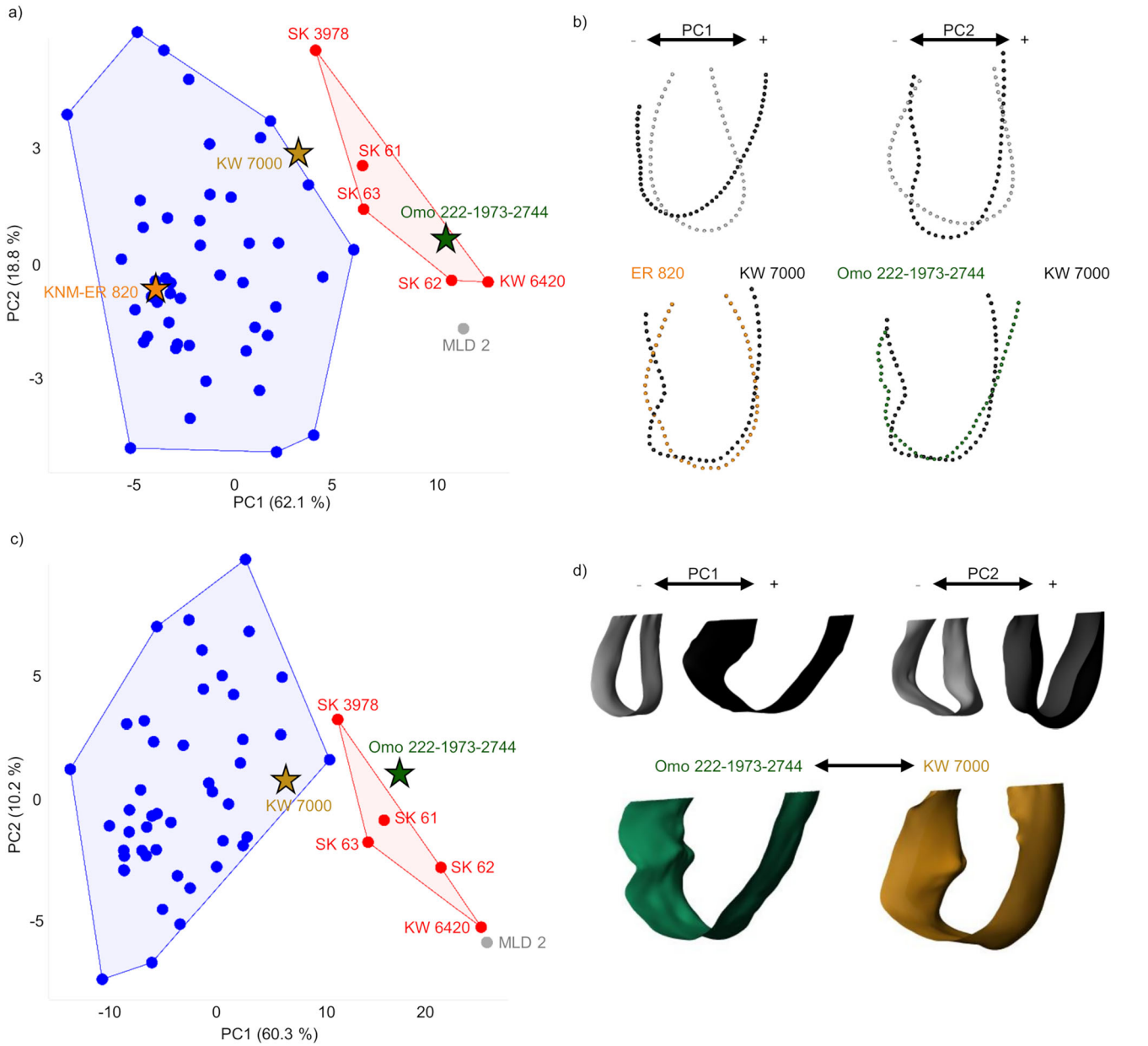

Fig. 7 | Morphometric comparisons of the KW 7000 mandibular symphysis with Omo 222-1973-2744, KNM-ER 820, *Paranthropus robustus*, *Australopithecus africanus* and *Homo sapiens* infants. The symphyseal shape is compared between KW 7000 (brown star), Omo 222-1973-2744 (dark green star), KNM-ER 820 (dark orange star), *P. robustus* infants (in red), *A. africanus* (in gray), and *H. sapiens* infants (in dark blue). **a** Plot of principal components (PCs) 1 and 2 illustrating the differences along the mid-sagittal plane of the symphysis. Variations within taxa are represented as convex polyhedra that enclose the corresponding points. **b** Configurations of 50 landmarks and semi-landmarks positioned along the mid-sagittal plane of the symphysis, with the anterior view oriented to the right, showing shape changes associated with PC1 and PC2. The transitions depict the difference between the lowest values of PC1 and PC2 (in gray) to the highest values along these PCs (in black). **c** Plot of principal components (PCs) 1 and 2 illustrating variations across the symphyseal surface. **d** Symphyseal surfaces interpolated from configurations of 120 evenly distributed landmarks and semi-landmarks to illustrate morphological differences, with the anterior view oriented to the right. These include contrasts along PC1 and PC2, and distinctions between Omo 222-1973-2744 (in dark green) and KW 7000 (in brown).

played an important role in generating phenotypic variation within early *Homo*[43]. However, environmentally-induced developmental variations alone cannot entirely account for the evolution of the juvenile skeleton in early *Homo*. This is because, in humans, the skull and adjacent skeletal elements are more developed at birth, making them less influenced by environmental factors compared to more distal structures (e.g., the lower limbs) that grow later and more rapidly[44,45]. These findings highlight the importance of further investigating infant craniofacial morphology in early *Homo* to better understand its influence on the phenotypic variation within this group.

We identify facial structural (i.e., shape) novelties in DNH 83, likely driven by evolutionary changes appearing early in craniofacial ontogeny in Early Pleistocene *Homo*. In the DNH 83 midface, these novelties include (i) the antero-posterior shortening (Fig. 2, Supplementary Figs. 3, 5, Supplementary Table 1) and (ii) early fusion of the premaxilla (Supplementary Fig. 4), as well as (iii) its posterior displacement relative to the nasal aperture (Fig. 2, Supplementary Fig. 5). When identified in the SK 847 adult specimen from Swartkrans (South Africa), these features have been regarded as derived traits compared to those of *Paranthropus* and *Australopithecus*[10,46]. Their presence in both the

https://doi.org/10.1038/s41467-025-59734-x

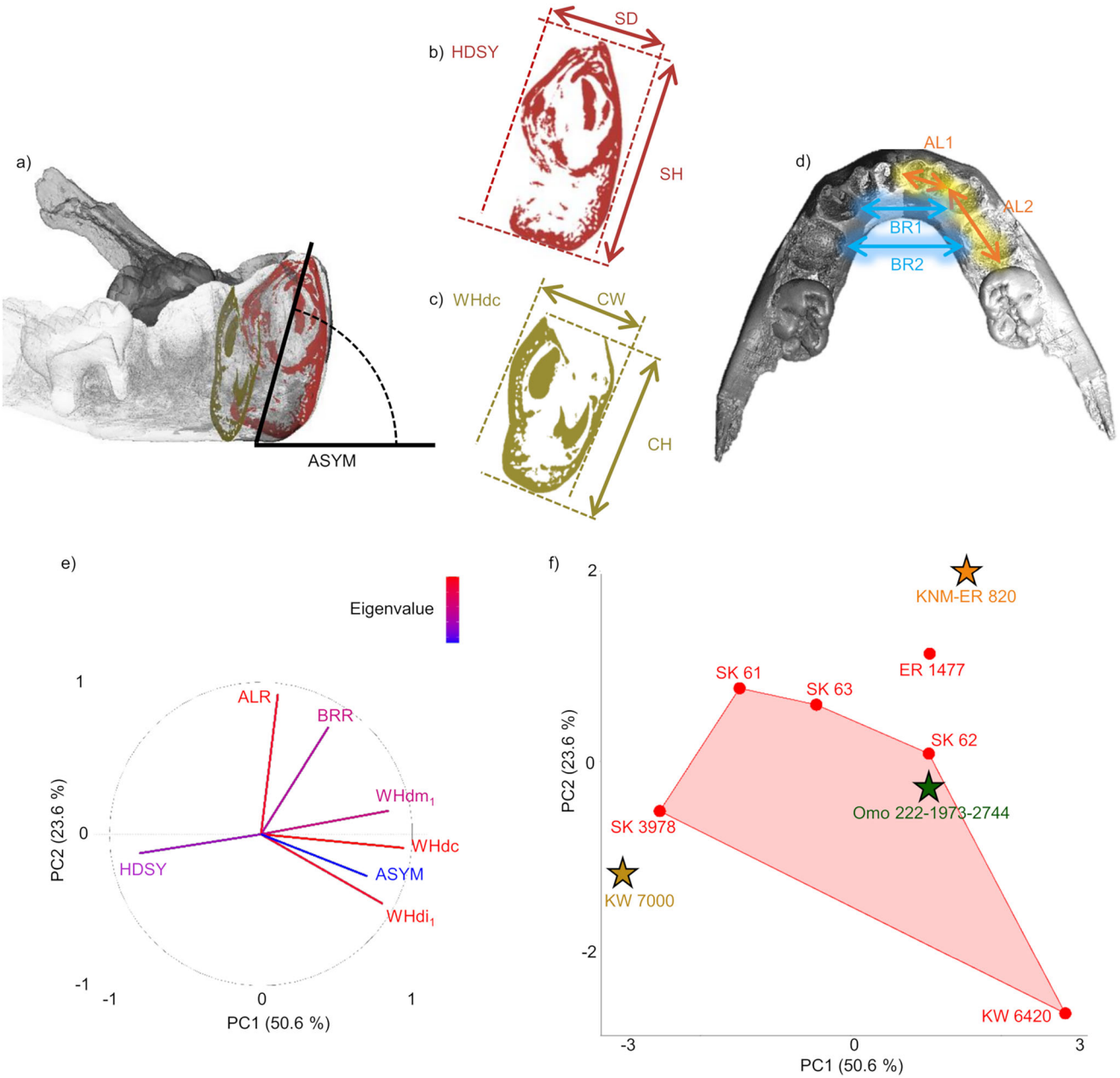

Fig. 8 | Morphometric comparisons of the KW 7000 mandible with Omo 222-1973-2744, KNM-ER 820, and *Paranthropus* infants. a A 3D rendering of the KW 7000 mandible in right lateral view, displayed in transparency, includes a mid-sagittal cross-section of its symphysis (**b**, highlighted in red, with the anterior view oriented to the right) and a cross-section of its corpus at the level of the deciduous canine (**c**, shown in yellow-green, with the lateral view oriented to the right). These illustrations demonstrate: **a** the angle between the symphyseal axis and the basal plane (ASYM), **b** the symphyseal height (SH), maximal depth (SD) and their index (HDSY = SD/SH), and **c** the corpus width (CW), height (CH) and the index (WHdc=CW/CH) at the level of the deciduous canine (dc). **d** A 3D rendering of the KW 7000 mandible in superior view, with the left side mirrored to the right, to illustrate measurements including: the minimum chord distance between the infradentale and the midpoint of the alveolar septum between the di_2 and dc (AL1), the minimum chord distance between the midpoint of the interalveolar septum between the di2/dc and the posterior wall of the dm_1 alveolus (AL2), and their ratio (ALR = AL1/AL2). Additionally, the minimum chord distances between the walls of the right and left dc alveoli (BR1), the walls of the right and left dm_1 alveoli (BR2), and their ratio (BRR = BR1/BR2) are also shown. **e**, **f** Principal component (PC) analysis of seven mandibular indices and one angle with **e** the correlation circle to illustrate how the eigenvalue of each variable is correlated to either PC1 or PC2, **f** a plot of PC1 and PC2 illustrating the differences between KW 7000 (brown star), Omo 222-1973-2744 (dark green star), KNM-ER 820 (dark orange star), *Paranthropus robustus* and *Paranthropus boisei* infants (in red). Variations within taxa are represented as convex polyhedra that enclose the corresponding points.

SK 847 adult and the DNH 83 infant suggest that the latter also possessed a derived midface, though confidently attributing it to an early *Homo* species remains challenging due to the lack of comparative material.

Further supporting the presence of evolutionary novelties in both the upper and lower facial regions, the mandible of KW 7000 exhibits two derived features that align with those observed in Early Pleistocene fossils, such as KNM-ER 820 attributed to *Homo* aff. *H. erectus*, and are distinct from *A. africanus*, *P. robustus,* and *P. boisei*: (i) the vertically inclined symphysis (Figs. 3 and 7, Supplementary Figs. 6 and 7) and (ii) geniohyoid depressions located more anteriorly on the inferior symphyseal surface (Fig. 3d, Supplementary Figs. 7, and 8). These two features likely form a functional module involving both the base of the mandible and the hyoid bone, a

https://doi.org/10.1038/s41467-025-59734-x

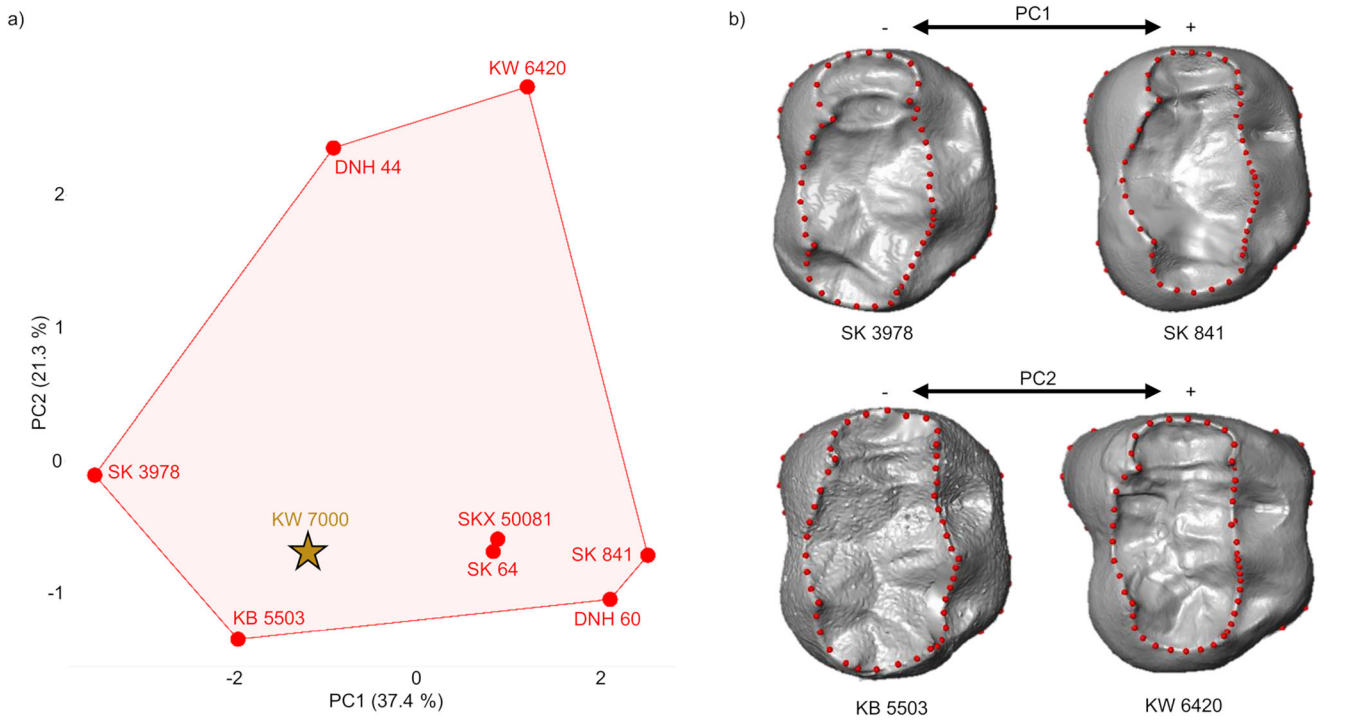

Fig. 9 | Morphometric comparisons of the KW 7000 dm_2 enamel-dentine junction with *Paranthropus robustus*. **a** Plot of principal components (PCs) 1 and 2 illustrating the variation in the configuration of 80 landmarks and semi-landmarks positioned on the dm_2 EDJ of KW 7000 (brown star) and *P. robustus* juveniles (in red). Variations within taxa are represented as convex polyhedra that enclose the corresponding points. **b** Differences in these dm_2 configurations are shown from the lowest values of PC1 (SK 3978) and PC2 (KB 5503) to the highest values along these respective PCs (SK 841 for PC1 and KW 6420 for PC2).

relationship supported by experimental studies[47], dissections of human cadavers[48], and comparisons between human and chimpanzee neonates and infants[42]. A key component in this functional system is the geniohyoid muscle, a small and short suprahyoid muscle involved in chewing, swallowing, and phonetics. The geniohyoid muscle inserts on the base of the mandible, and it has been shown that this insertion influences the anterior growth of the symphysis[47]. This influence is further emphasized by findings that the anterior displacement of the hyoid bone can occur with only the anterior displacement of the geniohyoid insertion[48]. Moreover, it was shown that in both humans and chimpanzees, the positioning of the hyoid bone relative to the inferior border of the symphysis is coordinated with the symphysis' orientation. In *H. sapiens*, the anterior displacement of the geniohyoid insertion is linked to the vertical inclination of the symphysis, whereas in chimpanzees, the posterior displacement of the geniohyoid insertion is associated with the symphysis' inclination[42]. This is consistent with the functional relationship between a more anterior placement of the geniohyoid insertion and the vertical inclination of the symphysis in the KW 7000 early *Homo* infant. Compared to *Paranthropus*, the symphyseal morphology of KW 7000 suggests a probable anterior displacement of the hyoid bone.

The morphology of KW 7000 is characterized by its vertically inclined symphysis and convex mental surface (Figs. 3 and 7a,b), as well as its gracile mandibular body (Fig. 8). Notably, unlike Omo 222-1973-2744, the shape of the KW 7000 symphysis falls within the range of variability observed in *H. sapiens* infants and older juveniles (Fig. 7). In contrast to Omo 222-1973-2744, the symphysis of KW 7000 more closely resembles that of the KNM-ER 820 *Homo* aff. *H. erectus* juvenile[38], which exhibits a similar symphysis, such as a prominent convex mental surface inferiorly (Fig. 7a, Supplementary Fig. 6), as originally described as a "mental trigon"[38]. Taking these comparisons into account, including the notable morphological difference between Omo 222-1973-2744 and KW 7000 (Supplementary Fig. 7), we propose assigning of KW 7000 to *Homo* aff. *H. erectus*.

The species designation of the Omo 222-1973-2744 juvenile is less clear when based solely on mandibular morphology. Compared to KW 7000, the more primitive gnathic features of Omo 222-1973-2744, both at the symphyseal (Figs. 4 and 7) and corpus levels (Figs. 4 and 8), align more closely with *P. robustus*. However, this observation needs to be nuanced, as the absence of infant mandibles attributed to both *H. habilis* and *H. rudolfensis* makes direct comparisons with Omo 222-1973-2744 and KW 7000 impossible. The mandibular corpus robusticity of Omo 222-1973-2744, indicated by high PC1 values in Fig. 8, closely resembles that of *P. robustus* and *P. boisei* infants, as well as the KNM-ER 820 *Homo* aff. *H. erectus* juvenile. The mandible of this latter specimen, unlike KW 7000, displays inconsistent taxonomic signals, with its derived symphysis suggesting affinity with *Homo* aff. *H. erectus* (Fig. 7), while its mandibular corpus robusticity index is closer to *P. boisei*. This discrepancy may be explained by the modular structure of the hominin mandible[49], and the impact of mechanical loading on the developmental changes in human corpus morphology[50]. This could also clarify why the KW 7000 infant (with its unerupted dm_2) and the developmentally older KNM-ER 820 juvenile (with its erupted M_1) differ in mandibular corpus robusticity, despite having similar symphyseal morphology. The older developmental age of Omo 222-1973-2744 (with its erupted dm_2) compared to KW 7000 may also contribute to differences in mandibular corpus robusticity. This trait is also distinctly expressed in the OH 7 *H. habilis* subadult, a species considered similar to *A. afarensis* in this regard[4]. Therefore, the mandibular corpus robusticity of Omo 222-1973-2744 does not necessarily indicate an attribution to *Paranthropus*. Unfortunately, the lower half of the symphysis in OH 7 is not preserved, preventing direct comparison with Omo 222-1973-2744, KW 7000, and KNM-ER 820 to determine whether it exhibited a primitive morphology in this region. Thus, the mandibular features of Omo 222-1973-2744 remain consistent with

its classification as *H. habilis*[31], supported by the morphology of its deciduous molars, where nine dental traits distinguish Omo 222-1973-2744 and other early *Homo* specimens from *P. boisei* (Supplementary Note 4). Additionally, the flat incisor row retracted along the bi-canine line, a defining feature of adult *H. rudolfensis*[5,7], is notably absent in both Omo 222-1973-2744 (Fig. 4c, d, Supplementary Fig. 6e and 7d) and KW 7000 (Fig. 3c, Supplementary Figs. 6a and 7c).

Fossil evidence of early *Homo* juvenile specimens from South Africa has been limited to very fragmented facial remains[51–53], isolated teeth[31], and the SK 54[30] and DNH 134[25] infant calvariae. The KW 7000 mandible from Kromdraai Unit P exhibits distinctly derived skeletal features characteristic of *Homo* (Figs. 7 and 8) but retains a primitive permanent canine morphology more akin *A. afarensis* (AL 400-1a,b)[39] and *A. africanus* (Sts 51)[40], while its dm_2 EDJ is indistinguishable from *P. robustus* (Fig. 9). This unique combination in KW 7000 infant provides valuable insights into the skeletal development of early *Homo* while emphasizing the need for caution when relying solely on isolated dental features[54] to assess the presence of early *Homo* in the early Pleistocene of South Africa. Notably, a similar and unique combination of derived skeletal morphology trending toward *H. erectus*[2,4] and more primitive overall dental morphology, akin to *Australopithecus* and certain early *Homo* specimens[14], was observed in the adult A.L. 666-1 maxilla from Hadar, Ethiopia, dated to 2.33 Ma[6]. Our confirmed attribution of Omo 222-1973-2744 to *H. habilis* suggests a derived deciduous molar morphology coupled with a more primitive mandibular structure. Therefore, the morphological differences between the mandibles of KW 7000 and Omo 222-1973-2744 (Fig. 7, Supplementary Fig. 7) indicate that taxonomic diversity in early *Homo* was evident as early as infancy, with skeletal and dental traits evolving independently.

The Early Pleistocene *Homo* record from southern Africa now appears to include diagnostic features of both the facial (KW 7000, DNH 83) and neurocranial (DNH 134[25], SK 54[30,55]) skeleton of juvenile specimens. Remarkably, DNH 83 and KW 7000 are the only infant specimens in this sample to combine both dental and skeletal evidence. Although the sample size is limited, this evidence highlights the importance of integrating dental and cranial morphology when evaluating the taxonomic affinities of individual early *Homo* specimens. More broadly, this highlights the need for extensive investigations with larger sample sizes to better understand the taxonomic significance of such dental and skeletal features within and across modern hominid subspecies and species. Additionally, developmental features, such as the early closure of the incisive suture, should play a more prominent role in classifying controversial specimens, such as StW 53 from Sterkfontein, which is considered either early *Homo*[56] or *Australopithecus*[46].

The comparative developmental evidence presented here suggests that *Homo* aff. *H. erectus* and *P. robustus* coexisted during the deposition of Unit P at the Kromdraai site, potentially before 2 Ma, as indicated by its bovid assemblage[27], pending confirmation through absolute dating. This conclusion is consistent with findings from Drimolen Main Quarry[25] and Swartkrans Member 1[10,51,52] assemblages, which also suggest that *Homo* aff. *erectus* was widespread and coexisted with *Paranthropus* in southern Africa around 2 Ma ago[25]. Understanding why early *Homo* infant remains are systematically less likely to be preserved than those of *P. robustus*, which often dominate the hominin assemblages (such as at Kromdraai Unit P)[36], is crucial to gaining broader insights into the paleoecology and behavior of these ancient taxa, and represents one of the most important questions to address in future research.

Methods

Permits

Original fossils from Drimolen Main Quarry (DMQ) (with the prefix DNH), Kromdraai Unit P (with the KW prefix) and Swartkrans (with the prefix SKW and SKX) are curated at the Evolutionary Studies Institute, University of the Witwatersrand in Johannesburg, South Africa, and researchers may apply for access through the University Fossil Access Advisory Committee by contacting the University Curator for Fossil and Rock Collections: Bernhard Zipfel, PhD, University Curator of Fossil and Rock Collections, Evolutionary Studies Institute, University of the Witwatersrand, Johannesburg (e-mail: Bernhard.Zipfel@wits.ac.za; Phone: +27-11 717-6683). For access to the original comparative fossils with the catalog prefixes STS and SK (from the sites of Sterkfontein and Swartkrans, respectively), these are curated at the Ditsong Museum of Natural History in Pretoria, South Africa, and researchers may apply for access to the Fossil Access Committee by contacting: Lazarus Kgasi, the Curator of Plio-Pleistocene Palaeotology, Ditsong Museums of South Africa (e-mail: lkgasi@ditsong.org.za; Phone: +27-12 492 5744). The KW 7000 specimen was recovered at the Kromdraai hominin site, under excavation permit IDs 2108 issued by the South African Heritage Resources Agency (SAHRA) to José Braga, in collaboration with Francis Thackeray. The specimens DNH 83 and DNH 84 were recovered under a permit for excavations at the Drimolen site, issued by SAHRA to André Keyser, in collaboration with Colin Menter.

Samples

All the original fossil hominin specimens presented in this study were examined with a low-power binocular microscope. One of us (JB) analyzed the fossils from Ethiopia and Kenya in 1996, while the specimens from South Africa have been studied continuously since the 1990s. The measurements were taken using a dial-equipped vernier caliper. All measurements are given in millimeters (mm) and were recorded to the nearest 0.1 mm when necessary. For damaged areas where it was possible to estimate a measurement with reasonable accuracy, it was recorded as 'circa' (c.).

The fossils from Kromdraai Unit P (KW 7000, KW 6420, KW 9000), Swartkrans (SK 3978, SK 62, SK 61, SK 63), Sterkfontein (STS 2), Makapansgat (MLD 2) and Taung (South Africa) were micro-CT scanned using the Nikon Metrology XTH 225/320 LC dual source industrial micro-CT system at the Palaeosciences Center in the University of the Witwatersrand (Johannesburg, South Africa), and the Metris X-Tek XT H225L at the South African Nuclear Energy Corporation (Pelinbada, South Africa), with isometric voxel dimensions ranging from 17.857 to 42.85 μm. The fossils from DMQ (DNH 47, DNH 83, DNH 44, and DNH 84) were scanned using X-ray synchrotron microtomography on beamline ID19 of the European Synchrotron Radiation Facility (Grenoble, France) with isometric voxel dimensions of 20.24 μm. The geometry of six fossils from East Africa was reconstructed from micro-CT scans of the original specimens. These fossils include KNM-ER 820, KNM-ER 1507, KNM-ER 1477, and KNM-ER 1820 from the National Museums of Kenya in Nairobi; Omo 222-1973-2744 from the National Museum of Ethiopia in Addis Ababa; and OH 7 from the National Museum of Tanzania in Dar es-Salaam. Data for the Kenyan specimens were sourced from the Human Fossil Record Archive (https://human-fossil-record.org/). The datasets for Omo 222-1973-2744 and OH 7 were kindly provided by Prof. Zeresenay Alemseged (Department of Organismal Biology and Anatomy, University of Chicago) and Prof. Fred Spoor (Center for Human Evolution Research, Natural History Museum, London, UK), respectively. All data were generated by the Department of Human Evolution at the Max Planck Institute for Evolutionary Anthropology (Leipzig, Germany) under the leadership of Prof. Jean-Jacques Hublin. The other micro-CT data used in this study are from the database of the Center for Anthropobiology and Genomics of Toulouse (France) (https://cagt.cnrs.fr/).

The comparative australopith specimens used for the morphological analysis of the KW 7000 canine include the following: for *A. afarensis*, A.L. 128-23, A.L. 198-1, A.L. 333w-58, A.L. 400-1a,b, as described in refs. 39,57; for *A. africanus*, Sts 50, Sts 51 as described in Robinson (1956), Stw 21, Stw 58, Stw 109, Stw 116, Stw 132, Stw 142, Stw

143, Stw 213, Stw 288, Stw 351, Stw 365, Stw 106c, Stw 412, Stw 446, Stw 491, Stw 537 as described in ref. 58.

The *H. sapiens* sample (Supplementary Data 3) consists of individuals aged from newborn/neonate to 84 months, originating from either France or South Africa. We received permission to access these samples, which have been utilized in previous studies and where additional information is available[59,60]. The sample from France includes juvenile individuals from both the "Institut d'Anatomie Normale et Pathologique" (IANP) at the University of Strasbourg and the "Clinique Pasteur" in Toulouse. The sample from the IANP consists of skeletons of individuals whose sex and age-at-death are documented (cataloged with the "Embr" prefix). This collection was primarily assembled by Professors HWG Waldeyer and G Schwalbe before 1918[61]. The skeletons were scanned using an Xtreme system (Scanco, Switzerland) at the "Institut de Médecine et de Physiologie Spatiales" in Toulouse, with an isometric voxel size of 0.041 mm. The sample from the Clinique Pasteur (cataloged with the "CPEnf" prefix) consists of CT scans collected retrospectively between 2012 and 2014, primarily to visualize the maxillary sinuses. Since these CT data were digital, anonymized, and collected retrospectively, no approval from a local ethical committee was necessary. The pixel size ranged from 0.46 to 0.52 mm, with a maximum slice thickness of 2 mm. The sample from South Africa includes skeletons of juvenile individuals whose sex and age-at-death are also documented, and sourced from the Dart collection (University of the Witwatersrand, Johannesburg, South Africa) and the Pretoria Formaline Collection (University of Pretoria, South Africa). These specimens were scanned using the X-Tek (Metris) XT H225L industrial CT system at the South African Nuclear Energy Corporation (NECSA, www.necsa.co.za), with isometric voxel sizes ranging from 0.04 mm to 0.1 mm.

3D data processing

We used the software Avizo, version 6.3 (Thermo Fisher Scientific; www.thermofisher.com) to process the X-ray synchrotron and micro-CT datasets. Our use of Avizo 6.3 adheres to the conditions outlined in the license provided to one of the authors (JB). Avizo 6.3 was employed for a range of advanced image processing tasks, including 3D surface reconstructions, spatial alignments, quantitative measurements, generation of 2D cross-sectional views, and segmentation of anatomical structures. The segmentation of the tooth germs was performed using a combination of manual tracing and semi-automated threshold-based techniques, allowing for precise delineation of tissue boundaries. Figures generated using Avizo 6.3 include Figs. 1–9, and Supplementary Figs. 1 and 3–9, which depict 3D renderings derived from the processed data.

Dental development

We recorded the formation of the deciduous and permanent teeth in all fossil hominins using a scale[62] that includes the following 14 successive developmental stages indicating the proportion of crown (Cr) and root (R) complete or resorbed: 0, no sign of crypt formation; 1, empty crypt; Ci, cusp(s) initiated; Cco, cusps coalescence; Crcco, crown outline complete; Cr1/2, crown 1/2; Cr3/4, crown 3/4; Crc, crown complete; Ri, root initiated; Cli, cleft initiated; R1/4, root 1/4; R1/2, root 1/2; R3/4, root 3/4; Rc, root complete; A, apex 1/2; Ac, apex complete. These calcification stages were assessed using micro-CT or X-ray synchrotron microtomography.

Morphometry

Regarding the maxilla, we used the following five measurements (Supplementary Table 1): (i) "anterior palatal breadth"[63] as the "distance between the lingual alveolar margins of the palate, measured at the most medial point on the septum between the canine and third premolar on either side" (p. 124 in ref. 63); (ii) "anterior maxillo-alveolar breadth"[61] as the "distance between the alveolar margins of the maxillae, measured at the outer margin of the septum between the canine and third premolar on either side" (p. 124 in ref. 63); (iii) "anterior premaxilla breadth" (APB) defined as the distance perpendicular to the sagittal plane, between, on the one hand, the outer margin of the septum between the lateral deciduous incisor and the deciduous canine, and, on the other hand, the midplane at the level of the inter-maxillary suture; (iv) "anterior alveolar length" (AAL) defined as the sum of the i1-dc mesiodistal alveolar lengths (chord distances); (v) "antero-posterior length of the premaxilla" (APLP)[30] as "measured between the prosthion and the center of the incisive foramen" (p. 3 in ref. 30). Regarding the mandible, we used the following 19 measurements, indices and angle (Supplementary Table 2): (i) "symphyseal height" (SH) or "minimal distance between the base of the symphysis and infradentale" (p. 295 in ref. 38), (ii) "symphyseal depth" (SD) or "maximal depth, at right angles to symphyseal height" (p. 295 in ref. 38) and (iii) the SD/SH ratio (HDSY) (Fig. 8b); (iv–vi) "corpus height" at di_1, dc and dm_1 (H) or "minimum distance between the most inferior point on the base and the lingual alveolar margin at the midpoint" of di_1, dc and dm_1 (p. 295 in ref. 38), (vii–ix) "corpus width" at di_1, dc and dm_1 (W) or "minimum width at right angles to [corpus height] taken at the midpoint of di1, dc and dm1 (p. 296 in ref. 38) and (x–xii) their W/H ratios ($WHdi_1$, WHdc and $WHdm_1$) (Fig. 8c); (xiii) the minimum chord distance between the infradentale and the midpoint of the alveolar septum between the di_2 and dc (AL1), (xiv) the minimum chord distance between the midpoint of the interalveolar septum between the di_2/d_c and the posterior wall of the dm_1 alveolus (AL2), and (xv) their ratio (ALR) (Fig. 8d); (xvi) the minimum chord distances between the walls of the right and left dc alveoli (BR1), (xvii) the minimum chord distances between the walls of the right and left dm_1 alveoli (BR2), and (xviii) their ratio (BRR) (Fig. 8d); (xix) the angle between the symphyseal ASYM (Fig. 8a).

In order to compare the maxillary (midfacial) morphology, we used on the right maxilla (or, in cases where it was not preserved, on a mirrored replica from the left maxilla), where we identified the following 3 landmarks and 20 semi-landmarks illustrated in Supplementary Fig. 9 and numbered as follows: (i) the prosthion (landmark 8) and 7 semi-landmarks (semi-landmarks 1–7) located from medial (adjacent to the prosthion) to lateral, along the buccal edge of the alveolar border, to the septum between the deciduous canine (d^c) and the first deciduous molar (dm^1); (ii) the prosthion (landmark 8) and 6 semi-landmarks positioned along the midline contour of the nasoalveolar clivus (semi-landmarks 9–14, clockwise); (iii) one landmark (landmark 15) at the base of the lateral margin of the nasal aperture; (iv) one landmark positioned at the lingual extremity of the septum between the right d^c and dm^1 (landmark 16) along with 7 semi-landmarks (semi-landmarks 17–23) positioned on the hard palate from lateral to medial. These 7 semi-landmarks numbered 17–23 lie on a vertical and transverse plane perpendicular to the alveolar border, extending to the midline. The intraobserver error of landmark placement on the maxilla was assessed by repeating this process (ten times by J.B.) on one *H. sapiens* infant. Within this (intra-individual) sample, the minimum, maximum, and mean Procrustes distances were always considerably lower (i.e., at least 16 times) than the (interindividual) minimum, maximum, and mean Procrustes distances for the total *H. sapiens* sample. Therefore, the intraobserver error in the placement of landmarks had a negligible effect on the results of our study.

To compare the symphysis, we used two configurations of landmarks and semi-landmarks. With the first configuration, we analyzed the area enclosed by the mesial faces of the left and right crowns of the deciduous or permanent canines, with the inferior boundary being the base of the alveolar bone to exclude the teeth. This area is hereafter called "symphyseal surface". In some fossil specimens, if one side was incomplete, it was reconstructed by mirroring the opposite side. The symphyseal surface does not provide

distinct anatomical features for reliably placing homologous landmarks. Therefore, we extracted automatically equidistantly spaced semi-landmarks on the symphyseal surface, as provided in Supplementary Data 1, using the protocol described in ref. 64. We briefly summarize the procedure here for convenience. First, on the mid-sagittal profile, we identified two key landmarks: the anterior and posterior infradentale, which are the midline points located between the central incisors at the front and back of the alveolar border, respectively. Next, we extracted a series of evenly spaced 2D slices—each containing a profile curve similar to the mid-sagittal profile. On each of these profile curves, including the mid-sagittal one, we extracted semi-landmarks, to capture the shape of the curves. Depending on the configuration, we used either 6 or 8 profile slices, and placed 10 or 15 semi-landmarks along each curve. This resulted in a total of either 60 or 120 landmarks and semi-landmarks used in two different analyses. Consistent with a previous study using this method and the same sample (excluding the KW 7000 specimen)[62], we obtained similar results when we used 60 or 120 landmarks and semi-landmarks to sample the symphyseal surface. In the second configuration, we utilized the infradentale anterior and posterior (as described above), along with 48 semi-landmarks automatically placed at equal intervals between them along the mid-sagittal plane of the symphysis.

A total of 80 3D landmarks and semi-landmarks were collected on the EDJ of the dm_2 as follows: (i) five landmarks were placed on the dentine horns of the five main cusps (in a clockwise sequence from the protoconid to the metaconid), with 45 semi-landmarks automatically distributed at equal intervals along the ridges connecting them; (ii) one landmark was positioned at the cemento-enamel junction on the mesiobuccal corner of the crown, just below the protoconid, followed by 29 semi-landmarks automatically placed at equal intervals along the same junction.

For each configuration of maxillary (midfacial), mandibular, and deciduous molar (dm_2) landmarks and semi-landmarks, we performed a GPA with scaling. All statistical analyses were assessed using the R packages "Morpho" version 4.0.5 (see https://cran.r-project.org/web/packages/Morpho/index.html) and "Geomorph" version 4.0.0 (see https://cran.r-project.org/package=geomorph). After Procrustes superimposition, we summarized variation in shape space using a PCA. We used a permutation test (or Monte-Carlo test, or randomization test) in the R "ade4 package" (see https://cran.r-project.org/web/packages/ade4/index.html) in order to assess the statistical significance of each PCA. The statistical significance was evaluated with a Monte-Carlo permutation test and the 'randtest.between' function by simulating 999 permutations. When we report significant differences in our PCAs, it indicates that the corresponding permutation test yielded significance with a p-value of less than 0.001. When applying this test to evaluate differences in symphyseal shape between KW 7000 and *H. sapiens* on one side, and Omo 222-1973-2744, *P. robustus*, and *A. africanus* on the other, we obtained p-values well below 0.001 for both Fig. 7a, c. We also used the function "plotRefToTarget" (package "Geomorph") to illustrate the shape differences between fossil specimens using vectors and warpings.

Reporting summary

Further information on research design is available in the Nature Portfolio Reporting Summary linked to this article.

Data availability

All data supporting this manuscript are available as Supplementary Data. Shape data used in the analyses are provided in Supplementary Data 1, while dental measurements are compiled in Supplementary Data 2. A detailed list of all individuals included in the study, along with their respective repositories and locations of deposition, is available in Supplementary Data 3. Access to the raw scan data must be requested directly from the relevant curatorial institutions and online archives, as specified in Supplementary Data 3. Data underlying all figures are included in Supplementary Data 1.

Code availability

The code used to reproduce all analyses and generate the figures is available in Supplementary Data 1.

References

1. Wood, B. & Collard, M. The human genus. *Science* **284**, 65–71 (1999).
2. Kimbel, W. H. & Villmoare, B. From *Australopithecus* to *Homo*: the transition that wasn't. *Philos. Trans. R. Soc. Lond. B Biol. Sci.* **371**, 20150248 (2016).
3. Wood, B. & Collard M. In *Handbook of Paleoanthropology* (eds. Henke, W. & Tattersall, I.) 1575–1610 (Springer, 2015).
4. Spoor, F. et al. Reconstructed *Homo habilis* type OH 7 suggests deep-rooted species diversity in early *Homo*. *Nature* **519**, 83–86 (2015).
5. Leakey, M. G. et al. New fossils from Koobi Fora in northern Kenya confirm taxonomic diversity in early *Homo*. *Nature* **488**, 201–204 (2012).
6. Kimbel, W. H., Johanson, D. C. & Rak, Y. Systematic assessment of a maxilla of *Homo* from Hadar, Ethiopia. *Am. J. Phys. Anthropol.* **103**, 235–262 (1997).
7. Spoor, F. et al. Implications of new early *Homo* fossils from Ileret, east of Lake Turkana, Kenya. *Nature* **448**, 688–691 (2007).
8. Suwa, G. et al. Early Pleistocene *Homo erectus* fossils from Konso, southern Ethiopia. *Anthropol. Sci.* **115**, 133–151 (2007).
9. Villmoare, B. et al. Arrowsmith, K.E. Reed, Early *Homo* at 2.8 Ma from Ledi-Geraru, Afar, Ethiopia. *Science* **347**, 1352–1355 (2015).
10. Clarke, R. J. *The Cranium Of The Swartkrans Hominid Sk 847 And Its Relevance To Human Origins*. PhD thesis, University of the Witwatersrand (1977).
11. Capraro, L. et al. The Monte San Nicola section (Sicily) revisited: a potential unit-stratotype of the Gelasian Stage. *Quat. Sci. Rev.* **278**, 107367 (2022).
12. Gabunia, L. et al. Earliest Pleistocene cranial remains from Dmanisi, republic of Georgia: taxonomy, geological setting, and age. *Science* **288**, 1019–1025 (2000).
13. Grine, F. E. et al. In *The first humans: origin of the genus* Homo (eds. Grine, F. E., Fleagle, J. G. Leakey, R. E.), 49-62 (Springer, 2009).
14. Rowan, J. et al. Early Pleistocene large mammals from Maka'amitalu, Hadar, lower Awash Valley, Ethiopia. *PeerJ* **10**, e13210 (2022).
15. Davies, T. W. et al. Dental morphology in *Homo habilis* and its implications for the evolution of early *Homo*. *Nat. Commun.* **15**, 286 (2024).
16. Leakey, L. S. B., Tobias, P. V. & Napier, J. R. A new species of the genus *Homo* from Olduvai Gorge. *Nature* **202**, 7–9 (1964).
17. West-Eberhard, M. J. Developmental plasticity and the origin of species differences. *Proc. Natl Acad. Sci. Usa.* **102**, 6543–6549 (2005).
18. Raff, R. A. *The shape of life. genes, development, and the evolution of animal form*. (University of Chicago Press, 1996).
19. Dean, M. C. et al. Growth processes in teeth distinguish modern humans from *Homo erectus* and earlier hominins. *Nature* **414**, 628–631 (2001).
20. Dean, M. C. & Smith, B. H. In *The first humans: origin of the genus* Homo (eds. Grine, F. E., Fleagle, J. G., Leakey, R.E.), 101–120 (Springer, 2009).
21. Dean, M. C. Measures of maturation in early fossil hominins: events at the first transition from australopiths to early *Homo*. *Philos. Trans. R. Soc. Lond. B Biol. Sci.* **371**, 20150234 (2016).
22. Smith, T. M. et al. Dental ontogeny in pliocene and early pleistocene hominins. *PLoS One* **10**, e0118118 (2015).

23. Zollikofer, C. P. E. et al. Dental evidence for extended growth in early *Homo* from Dmanisi. *Nature* **635**, 906–911 (2024).
24. Tacail, T. et al. Calcium isotopic patterns in enamel reflect different nursing behaviors among South African early hominins. *Sci. Adv.* **5**, eaax3250 (2019).
25. Herries, A. I. R. et al. Contemporaneity of *Australopithecus*, *Paranthropus*, and early *Homo erectus* in South Africa. *Science* **368**, eaaw7293 (2020).
26. Pickering, R., Kramers, J. D., Hancox, P. J., de Ruiter, D. J. & Woodhead, J. D. Contemporary flowstone development links early hominin bearing cave deposits in South Africa. *Earth Planet. Sci. Lett.* **306**, 23–32 (2011).
27. Hanon, R. et al. New fossil Bovidae (Mammalia: Artiodactyla) from Kromdraai Unit P, South Africa and their implication for biochronology and hominin palaeoecology. *Quat. Sci. Rev.* **331**, 108621 (2024).
28. Howell, F. C. & Coppens, Y. In *Earliest Man and Environments in the Lake Rudolf Basin* (eds Coppens, Y., Howell, F. C., Isaac, G. L. & Leakey R. E. F.) 522–532 (University of Chicago Press, 1976).
29. Feibel, C. S., Brown, F. H. & McDougall, I. Stratigraphic context of fossil hominids from the Omo group deposits: northern Turkana Basin, Kenya and Ethiopia. *Am. J. Phys. Anthropol.* **78**, 595–622 (1989).
30. Braga, J. et al. Hominin fossils from Kromdraai and Drimolen inform *Paranthropus robustus* craniofacial ontogeny. *Sci. Adv.* **9**, eade7165 (2023).
31. Grine, F. E. *The deciduous dentition of the Kalahari San, the South African negro and the South African Plio-Pleistocene hominids*, PhD thesis, University of the Witwatersrand (1984).
32. Tobias, P. V. *Olduvai Gorge Volume 4: The Skulls and Endocasts of* Homo habilis (Cambridge University Press, 1991).
33. Maureille, B. & Braga, J. In *Human Evolution Through Developmental Change* (eds. Minugh-Purvis, N. & McNamara, K.) 464–478 (The Johns Hopkins University Press, 2002).
34. Scheuer, L. & Black, S. *Developmental Juvenile Osteology* (Academic Press, 2000).
35. Rak, Y. *The Australopithecine Face* (Academic Press, 1983).
36. Braga, J. & Grine, F. E. New craniodental fossils of *Paranthropus robustus* from Kromdraai, South Africa (2014-2017 excavations). *J. Hum. Evol.* **188**, 103481 (2024).
37. Grine, F. E. New hominid fossils from the swartkrans formation (1979-1986 excavations): craniodental specimens. *Am. J. Phys. Anthropol.* **79**, 409–449 (1989).
38. Wood, B. Koobi Fora Research Project. Volume 4: Hominid cranial remains (Clarendon Press, 1991).
39. Johanson, D. C., White, T. D. & Coppens, Y. Dental remains from the Hadar Formation, Ethiopia: 1974-1977 collections. *Am. J. Phys. Anthropol.* **57**, 545–603 (1982).
40. Robinson, J. T. The dentition of the Australopithecinae. *Transvaal Mus. Mem.* **9**, 1–179 (1956).
41. Dart, R. A. *Australopithecus africanus*: the man-ape of South Africa. *Nature* **115**, 195–199 (1925).
42. Coquerelle, M., Bookstein, F. L., Braga, J., Halazonetis, D. J. & Weber, G. W. Fetal and infant growth patterns of the mandibular symphysis in modern humans and chimpanzees (*Pan troglodytes*). *J. Anat.* **217**, 507–520 (2010).
43. Antón, S. C. & Kuzawa, C. W. Early *Homo*, plasticity and the extended evolutionary synthesis. *Interface Focus* **7**, 20170004 (2017).
44. Eveleth, P. B. & Tanner, J. M. *Worldwide variation in human growth* (Cambridge University Press, 1990).
45. Bogin, B. *Patterns of human growth* (Cambridge University Press, 1999).
46. Braga, J. Chimpanzee variation facilitates the interpretation of the incisive suture closure in South African Plio-Pleistocene hominids. *Am. J. Phys. Anthropol.* **105**, 121–135 (1998).
47. Spyropoulos, M. N., Tsolakis, A. I., Alexandridis, C., Katsavrias, E. & Dontas, I. Role of suprahyoid musculature on mandibular morphology and growth orientation in rats. *Am. J. Orthod. Dentofac. Orthop.* **122**, 392–400 (2002).
48. Kutzner, E. A. et al. Effect of genioglossus, geniohyoid, and digastric advancement on tongue base and hyoid position. *Laryngoscope* **127**, 1938–1942 (2017).
49. Jung, H., Strait, D., Rolian, C. & Baab, K. L. Evaluating modularity in the hominine skull related to feeding biomechanics. *Am. J. Biol. Anthropol.* **183**, 39–59 (2024).
50. Holmes, M. A. & Ruff, C. B. Dietary effects on development of the human mandibular corpus. *Am. J. Phys. Anthropol.* **145**, 615–628 (2011).
51. Grine, F. E. & Strait, D. S. New hominid fossils from Member 1 "hanging remnant," Swartkrans formation, South Africa. *J. Hum. Evol.* **26**, 57–75 (1994).
52. Grine, F. E. Early *Homo* at Swartkrans, South Africa: a review of the evidence and an evaluation of recently proposed morphs. *S. Afr. J. Sci.* **101**, 43–52 (2005).
53. Moggi-Cecchi, J., Tobias, P. V. & Beynon, A. D. The mixed dentition and associated skull fragments of a juvenile fossil hominid from Sterkfontein, South Africa. *Am. J. Phys. Anthropol.* **106**, 425–465 (1998).
54. Zanolli, C. et al. Dental data challenge the ubiquitous presence of *Homo* in the Cradle of Humankind. *Proc. Natl. Acad. Sci. USA* **119**, e2111212119 (2022).
55. Brain, C. K. New finds at the Swartkrans australopithecine site. *Nature* **225**, 1112–1119 (1970).
56. Curnoe, D. A review of early *Homo* in southern Africa focusing on cranial, mandibular and dental remains, with the description of a new species (*Homo gautengensis* sp. nov.). *Homo* **61**, 151–177 (2020).
57. Johanson, D. C., White, T. D. & Coppens, Y. A new species of the genus *Australopithecus* (Primates: Hominidae) from the Pliocene of eastern Africa. *Kirtlandia* **28**, 1–14 (1978).
58. Moggi-Cecchi, J., Grine, F. E. & Tobias, P. V. Early hominid dental remains from Members 4 and 5 of the Sterkfontein Formation (1966 - 1996 excavations): catalogue, individual associations, morphological descriptions and initial metrical analysis. *J. Hum. Evol.* **50**, 239–328 (2006).
59. Braga, J. et al. Cochlear shape reveals that the human organ of hearing is sex-typed from birth. *Sci. Rep.* **9**, 10889 (2019).
60. Braga, J. & Treil, J. Estimation of pediatric skeletal age using geometric morphometrics and three-dimensional cranial size changes. *Int. J. Leg. Med.* **121**, 439–443 (2007).
61. Rampont, M. Les squelettes, os, et dents de foetus, nouveaux-nés, et enfants du Musée Anatomique de Strasbourg. Aspects historiques et catalogue, PhD thesis, University of Strasbourg (1994).
62. Moorrees, C. F., Fanning, E. A. & Hunt, E. E. Age variation of formation stages for the permanent teeth. *J. Dent. Res.* **42**, 1490–1502 (1963).
63. Lockwood, C. A. Sexual dimorphism in the face of *Australopithecus africanus*. *Am. J. Phys. Anthropol.* **108**, 97–127 (1999).
64. Zimmer, V. A. et al. Revisiting mandibular symphyseal shape in juvenile early hominins and modern humans using a deformation-based approach. *Folia Primatol.* **94**, 225–247 (2023).

Acknowledgements

We dedicate this paper to the late Charles Lockwood. We thank the Lotz family, the South African Heritage Resources Agency, and the Cradle of Humankind World Heritage Management Authority for supporting fieldwork at Kromdraai (excavation permits ID: 3035, 3176, and 3888, J. Braga in collaboration with B. Zipfel and F. Thackeray). The Drimolen excavation was funded by the National Research Foundation (African Origin Platform, C. Menter). We thank the Evolutionary Studies Institute,

University of the Witwatersrand (B. Zipfel and S. Jirah) and the Ditsong National Museum of Natural History (S. Potze, L. Kgasi) for fossil access. We thank F. de Beer, J. Hoffman (South African Nuclear Energy Corporation), K. Jakata (University of the Witwatersrand), and P. Tafforeau (European Synchrotron Facility (Grenoble, France) for micro-CT or synchrotron scanning support. Finally, we thank V. Zimmer for technical support, Z. Alemseged and F. Spoor for sharing data on Omo 222-1973-2744 and OH 7, respectively. Funding was provided by the *Ministère de l'Europe et des Affaires Etrangères, Commission consultative des recherches archéologiques à l'étranger*, France (JB), the *Ministero degli Affari Esteri e della cooperazione internazionale. Missioni Archeologiche all'estero* (2006—2016), Italy (JMC), Erasmus Mundus Partnerships (AESOP and AESOP+, JB), the *Center National de la Recherche Scientifique, France* (JB), and the *Institut des Déserts et des Steppes*, France (JB).

Author contributions

J.B. and J.M.C. collected data, performed analyses, and wrote the paper.

Competing interests

The authors declare no competing interests.

Additional information

Supplementary information The online version contains supplementary material available at https://doi.org/10.1038/s41467-025-59734-x.

Correspondence and requests for materials should be addressed to José Braga.

Peer review information *Nature Communications* thanks Kevin Kuykendall, and the other, anonymous, reviewer(s) for their contribution to the peer review of this work. A peer review file is available.